Probing protein ubiquitination in live cells

Weihua Qin [1,*]**, Clemens Steinek**[1]**, Ksenia Kolobynina**[2]**, Ignasi Forné**[3]**, Axel Imhof** [3]**,**
M. Cristina Cardoso [2] **and Heinrich Leonhardt** [1,*]

[1]Faculty of Biology, Ludwig-Maximilians-Universität München, Großhaderner Str. 2, 82152 Planegg-Martinsried, Germany, [2]Cell Biology and Epigenetics, Department of Biology, Technical University of Darmstadt, Schnittspahnstr. 10, 64287 Darmstadt, Germany and [3]Biomedical Center Munich, Faculty of Medicine, Ludwig-Maximilians-Universität München, Großhaderner Str. 9, 82152 Planegg-Martinsried, Germany

ABSTRACT

The reversible attachment of ubiquitin governs the interaction, activity and degradation of proteins whereby the type and target of this conjugation determine the biological response. The investigation of this complex and multi-faceted protein ubiquitination mostly relies on painstaking biochemical analyses. Here, we employ recombinant binding domains to probe the ubiquitination of proteins in living cells. We immobilize GFP-fused proteins of interest at a distinct cellular structure and detect their ubiquitination state with red fluorescent ubiquitin binders. With this ubiquitin fluorescent three-hybrid (ubiF3H) assay we identified HP1β as a novel ubiquitination target of UHRF1. The use of linkage specific ubiquitin binding domains enabled the discrimination of K48 and K63 linked protein ubiquitination. To enhance signal-to-noise ratio, we implemented fluorescence complementation (ubiF3Hc) with split YFP. Using in addition a cell cycle marker we could show that HP1β is mostly ubiquitinated by UHRF1 during S phase and deubiquitinated by the protease USP7. With this complementation assay we could also directly detect the ubiquitination of the tumor suppressor p53 and monitor its inhibition by the anti-cancer drug Nutlin-3. Altogether, we demonstrate the utility of the ubiF3H assay to probe the ubiquitination of specific proteins and to screen for ligases, proteases and small molecules controlling this posttranslational modification.

INTRODUCTION

Protein ubiquitination is a highly conserved posttranslational modification which involves the concerted action of E1, E2 and E3 enzymes to ultimately ligate the carboxyl terminus of ubiquitin to a lysine residue of the selected protein target (1–3). Proteins can be modified at one or multiple lysine residues with a single ubiquitin or ubiquitin chains formed through one of their lysine residues (K6, K11, K27, K29, K33, K48 and K63) or the N-terminal methionine residue (M1). The K48-linked ubiquitin linkage predominantly signals for proteasomal degradation, whereas the K63-linked linkage is mainly involved in non-degradative processes such as DNA repair and NF-κB signaling (2,3). Due to technical challenges and difficulties in the detection of the other types of ubiquitin chains, less information is available about their functions. Since E3 ligases widely control protein levels and function, it becomes increasingly important to identify and characterize their specific targets in order to comprehend their unique contribution to complex regulatory protein networks.

The major approach for substrate identification relies on the physical interaction between a ubiquitin E3 ligase and its substrates, using methods such as yeast two-hybrid (Y2H), protein microarrays and biotin-dependent proximity labelling (BioID) (4–6). The ubiquitination of substrates has been directly monitored with donor/acceptor fluorophore pairs and sophisticated fluorescence resonance energy transfer (FRET) and fluorescence lifetime imaging (FLIM) techniques (7,8). Likewise, ubiquitin conjugation was detected with bimolecular complementation of fluorescence or luminescence (9,10) and was used for genetic screens (11). An alternative approach is to assay for altered protein stability upon chemical or genetic interference with an E3 ubiquitin ligase of interest as ubiquitinated proteins are targeted to proteasomal degradation (12,13), which could also be monitored by bioluminescence energy transfer (BRET) in PROTAC treated cells (14). Still, the gold standard in the identification of ubiquitination targets is mass spectrometry but, as a prominent biological function of this modification is proteasomal degradation, the fleeting abundance of modified target proteins often limits their detection.

To enrich for low abundance peptides from ubiquitinated proteins, antibodies that recognize the ubiquitin remnant

---

*To whom correspondence should be addressed. Tel: +49 89 2180 74232; Fax: +49 89 2180 74236; Email: h.leonhardt@lmu.de
Correspondence may also be addressed to Weihua Qin. Tel: +49 89 2180 71132; Fax: +49 89 2180 74236; Email: weihua@zi.biologie.uni-muenchen.de

motif Lys-e-Gly-Gly (diGly), which is exposed upon tryptic digestion of ubiquitinated proteins, have been developed for global proteomic applications (15–17). In addition, substrate trapping approaches based on polyubiquitin-binding domain fusions have been generated for the isolation of polyubiquitinated proteins from cell extracts (18,19). In contrast to antibodies, these ubiquitin-binding domains, which show different binding affinities for distinct ubiquitin linkages (20,21), can also be fused to fluorescent proteins to detect different biological ubiquitin signals (22–24). Similarly, GFP-tagged ubiquitin has been used to visualize free and linked ubiquitin in cells (25). While these methods detect general ubiquitination levels and proteome-wide changes (26,27), they do not allow to monitor ubiquitination of specific targets in live cells with spatio-temporal resolution.

The detection of specific protein ubiquitination in live cells requires a genetically encoded probe that specifically binds but ideally does not interfere with biological function. Here, we generated recombinant probes consisting of tandem ubiquitin association (2UBA) domains, or ubiquitin interacting motifs (2UIM) or a Npl4 zinc finger (NZF) fused to mCherry. These probes could detect local changes in protein ubiquitination, e.g. at cellular DNA repair foci. To detect the ubiquitination level of specific proteins we immobilized them at defined subcellular sites in a ubiquitin fluorescent-three-hybrid (ubiF3H) assay. The combination of the three ubiquitin probes could reveal the ubiquitination status of specific proteins in live cells. To enhance the signal-to-noise ratio we implemented and validated a protein complementation assay (PCA) that only generates a fluorescent signal if the protein of interest (POI) is ubiquitinated. This versatile tool set is suitable for high-throughput screens to identify E3 ligases and ubiquitin proteases in essentially any organism and to monitor changes over time and throughout the cell cycle.

MATERIALS AND METHODS

Expression constructs

The coding sequence of the UBA domain of RAD23 (amino acids 158 to 212), the NZF domain of TAB2 (amino acids 663–693) and the 2UIM domain of USP25 (amino acids 97–140) was amplified using cDNA from mouse embryonic stem cells (mESCs) E14. To generate the GFP-2UBA and Ch-2UBA constructs, a duplicate UBA coding sequence was subcloned into both the pCAG-GFP-IB and the pCAG-Ch-IB vector. The generation of expression constructs for Ch-USP7 (wt, full length), Ch-USP7^{C224S}, GFP-H3, GFP-PAF15, GFP-DNMT1, GFP-DNMT3A and HA-Ub was described previously (28–30). The human UHRF1 cDNA was ligated into pcDNA3.1 vector with EcoRI and HindII. To generate the GFP-HP1α, GFP-HP1β and GFP-HP1γ constructs, the HP1α, HP1β, HP1β^{delC} and HP1γ coding sequences were amplified using cDNA from mESCs and subcloned into pCAG-GFP-IB vectors.

The DNA sequence coding for full length of p21 and Cyclin B1 was amplified from mouse cDNA by PCR using Phusion high-fidelity DNA Polymerase (New England BioLabs) and cloned in frame into mCherry plasmid with AsiSI and NotI restriction endonucleases (New England BioLabs).

The mammalian expression constructs for RFP tagged PCNA, human p53, pGBP-lacI and pGBP-Lamin B1 were described previously (31–33). The GBP used in this study is GBP1, also termed as 'enhancer' (34).

The 2UBA was subcloned to fuse with YN (1–154) by a 4 × GGSG linker. Protein coding sequences including H3, PAF15, p53 and HP1β carrying AsiSI and NotI restriction cutting sites were subcloned to fuse with YC (155–235) by a 4 × GGSG linker.

All constructs (Supplementary Table S1) were verified by DNA sequencing.

Cell culture, transfection, inhibitor treatment and cell line generation

HEK293T, baby hamster kidney (BHK) cells carrying lac repressor/operator array (35), HeLa and mESCs were cultured and transfected as described previously (29,36), with the exception that Lipofectamine 3000 (Invitrogen) was used for the transfection of mESCs. For the *in vivo* ubiquitination assay, transfected HEK293T cells were incubated with medium supplemented with 2 mM *N*-ethylmaleimide (NEM) for 30 min before harvesting. For Nutlin-3 treatment, before transfection Nutlin-3 was added into the medium and incubated for ∼16 hours. For cell cycle analysis, mESCs were cultured in a medium containing 0.8 mM mimosine (37,38) for 24 h. Synchronized cells were then released into the cell cycle by adding fresh medium after washing once with medium. At different time points, samples were harvested for both WB analysis and flow cytometry (Aria II, Becton Dickinson). In brief, cells were washed twice with phosphate buffered saline (PBS), fixed with 70% ethanol for 15 min on ice and finally stained for 40 min at 37°C in solution containing 50 μg/ml propidium iodide (PI), 0.1 mg/ml RNase A, 0.05% Triton X-100. After washing once with PBS, the cell cycle profile was analyzed by flow cytometry.

The human cervical carcinoma HeLa Kyoto cells (ATCC No. CCL-2), HeLa Kyoto GFP-PCNA cells were grown in DMEM medium supplemented with 10% FCS, L-glutamine, and antibiotics at 37°C in a humidified atmosphere of 5% CO2. HeLa Kyoto cell lines expressing fluorescent PCNA variants were generated (39) using the Flp-In site-specific recombination system. HeLa Kyoto Ch-NZF, Ch-2UBA and Ch-2UIM cells were obtained by transfection with the plasmids bearing mCherry gene and NZF, 2UBA, 2UIM genes respectively. Positively transfected cells were selected visually. Cells were seeded on the μ-Dish35 mm (cat.no 81158, ibidi) in a concentration of 200.000 cells per dish. Cells were incubated for 24 h after transfection as described above.

Generation of cell lines stably expressing POIs was previously described (40). To generate YC-HP1β wt and YC-HP1β^{delC} BHK cells, 100 000 cells were plated in a 6-well plate and transfected with 2 μg of plasmid with Lipofectamine 3000 (Invitrogen) 2 h after plating. Cells were trypsinized 48 h after transfection and 5000 cells were plated in a p100 dish with a selection medium containing 10 μg/ml of blasticidin. One week later, 5000 cells were plated in a

new p100 dish with 10 μg/ml of blasticidin and cultured for another week. The HP1β antibodies (Abcam, ab10811) recognize the C-terminus and hence not the HP1β^{delC}, thus, the sequences coding for YC were amplified from genomic DNA using the primers listed in the Supplementary Table S1 to characterize those cell lines.

To stably express YC-HP1β wt and YC-PAF15 in mESCs, 100 000 cells were plated in a 6-well plate and transfected with 2 μg of plasmid with Lipofectamine 3000 (Invitrogen) after cells attached to the culture dish. 48 h after transfection, cells were trypsinized and plated into a p100 dish at a colony density with selection medium containing 10 μg/ml of blasticidin. 8 days after selection, colonies were picked. To characterize YC-HP1β wt and YC-PAF15 mESCs, western blot (WB) was performed with a polyclonal anti-HP1β and a monoclonal anti-PAF15 antibodies, respectively (see details in Supplementary Table S1).

Identification of UHRF1 targets

SILAC labeling of mESCs was performed at 37°C in ESCs medium supplemented with 100 μg/ml of light (L) or heavy (H) arginine and lysine isotopes, for L: Arg0 and Lys0 (L-arginine and L-lysine, Sigma-Aldrich), for H: Arg10 and Lys8 (arginine-13C6, 15N4 and lysine-13C6, 15N2, Silantes). In addition to the specific lysine and arginine, the completed ESC medium contained knockout DMEM (Silantes), 10% dialyzed serum, 6% knockout serum replacement, 2 mM L-glutamine, 0.1 mM non-essential amino acids, 50 μM 2-mercaptoethanol, 1000 units/ml leukemia inhibitory factor LIF, 1 μM MEK inhibitor PD and 3 μM GSK-3 inhibitor CHIR (2i, Axon Medchem). To assess the SILAC labeling efficiency, cells were cultured in SILAC medium for 10 passages and tested by MS. For identification of the targets, mESCs were first transfected with an expression vector for GFP-2UBA, the immunoprecipitation assay was then conducted as described below with minor modifications. Wt and *Uhrf1*-deficient cells were lysed in buffer containing 150 mM NaCl, 10 mM Tris–HCl (pH7.5), 2.5 mM MgCl$_2$, 2 mM phenylmethylsulphonyl fluoride and 0.5% NP-40, 1× Protease Inhibitor (Serva) and 1 μg/ul DNAse on ice for 30 min and cleared by centrifugation (20 000g for 15 min) at 4°C. Protein concentrations of cleared cell lysates were measured using the PierceTM 660 nm protein assay kit. Equal amounts (∼500 μg) of cell extracts were combined and incubated with the GFP-Trap for 2 h at 4°C under gentle rotation. The samples were separated by SDS-PAGE and prepared for LC–MS/MS as described (41). As a control, 500 μg of cell extracts from *Uhrf1*-deficient mESCs (light) expressing GFP were equally mixed with clear cell lysates from *Uhrf1*-deficient mESCs (heavy) expressing GFP-2UBA for immunoprecipitation with the GFP-Trap.

A standardized protocol was used for in-gel digestion with minor modifications (42,43). The digested peptides were evaporated to 5 μl and re-suspended in 30 μl of 0.1% TFA solution prior to desalting by C18 Stage tips. Samples were evaporated to dryness and re-suspended in 30 μl of 0.1% formic acid solution and stored at –20°C until LC–MS analysis. For LC–MS/MS purposes, desalted peptides were injected in an Ultimate 3000 RSLCnano system (Thermo),

separated in a 15-cm analytical column (75 μm ID with ReproSil-Pur C18-AQ 2.4 μm from Dr Maisch) with a 50 min gradient from 5 to 60% acetonitrile in 0.1% formic acid. The effluent from the HPLC was directly electrosprayed into a LTQ Orbitrap XL mass spectrometer (Thermo). The MS instrument was operated in a data dependent mode to automatically switch between full scan MS and MS/MS acquisition. Survey full scan MS spectra (from m/z 300–2000) were acquired in the Orbitrap with a resolution of $R = 60$ 000 at m/z 400 (after accumulation to a 'target value' of 500,000 in the linear ion trap). The six most intense peptide ions with charge state between 2 and 4 were sequentially isolated to a target value of 10 000 and fragmented in the linear ion trap by collision induced dissociation (CID). For all measurements with the Orbitrap mass analyzer, three lock-mass ions from ambient air (m/z = 371.10123, 445.12002, 519.13882) were used for internal calibration. Usual MS conditions were: spray voltage, 1.5 kV; no sheath and auxiliary gas flow; heated capillary temperature, 200°C; normalized collision energy 35% for CID in LTQ. The threshold for ion selection was 10 000 counts for MS2. MaxQuant 1.2.2.5 was used to identify proteins and quantify with the following parameters: Database, ipi.MOUSE.v3.68.fasta; MS tol, 10ppm; MS/MS tol, 0.5 Da; Peptide FDR, 0.1; Protein FDR, 0.01 min. peptide length, 5; variable modifications, oxidation (*M*); fixed modifications, carbamidomethyl (C); peptides for protein quantitation, razor and unique; min. peptides, 1; min. ratio count, 2.

Live-cell DNA damage assay

Live-cell DNA damage assay was carried out as previously described (44). Imaging and microirradiation experiments were performed using a Leica TCS SP5II confocal laser scanning microscope (Leica Microsystems, Wetzlar, Germany) equipped with an oil immersion Plan-Apochromat ×100/1.44 NA objective lens (pixel size in XY set to 76 nm) and laser lines at 405, 488, 561 and 633 nm. All imaging was conducted in a closed live-cell microscopy chamber (ACU, Olympus) at 37°C with 5% CO$_2$ and 60% humidity, mounted on the Leica TCS SP5II microscope. The emission of GFP and mCherry was captured using the detection range 495–549 and 610–680, respectively. For standard microirradiation, a preselected spot in non-S phase cells (1 μm diameter) within the nucleus was microirradiated for 0.6 s with the laser lines 405, 488, 561 nm laser set to 100%, or for 1.5 s with the laser lines 488 and 561 nm laser set to 100%. Before and after microirradiation, confocal image series of one mid nucleus z-section were recorded in 15 s intervals.

Photobleaching of mCh-NZF, mCh-2UBA or mCh-2UIM at previously microirradiated spots was performed using a circular region of interest (1 μm diameter) for 1 s with a 561 nm laser set to 100%. Before and after microirradiation and photobleaching, a confocal image series of one mid-nuclear z-section was recorded in 15 s intervals.

All analysis steps for the confocal microscopy images from microirradiation experiments were performed using ImageJ (45,46). Images were first corrected for cell movement and subsequently mean intensity of the irradiated region was divided by the mean intensity of the whole nu-

cleus (both corrected for background) using ImageJ software. For each experimental condition at least 25 cells were used. Half-times for ubiquitin probes accumulation were calculated from the time of microirradiation till maximal accumulation with one phase association (single exponential function: $Y = Y0 + (\text{Plateau} - Y0) \times (1 - e(-K \times X))$.

FRAP data were normalized by pre bleach fluorescence intensity. All fits were performed on averaged normalized FRAP curves and the resulting fit parameters are reported as the mean $\pm$ SEM for two or three independent experiments. Curve fitting was done to double the exponential equation.

Fluorescence loss in photobleaching (FLIP)

Fluorescence loss in photobleaching (FLIP) experiments were conducted using a Nikon TiE microscope equipped with a Yokogawa CSU-W1 spinning-disk confocal unit (50 µm pinhole size), an Andor Borealis illumination unit, Andor ALC600 laser beam combiner (405 nm/488 nm/561 nm/640 nm), Andor IXON 888 Ultra EMCCD camera, Andor FRAPPA photobleaching module, and a Nikon $100\times/1.45$ NA oil immersion objective. The microscope was controlled by software from Nikon (NIS Elements, ver. 5.02.00). Cells were transfected for 24 hours, plated on bottom 2-well imaging slides (Ibidi) and maintained at 37°C with 5% CO2 using an environmental chamber (Oko Labs). Pre-bleach images were acquired with the 488 nm and 561 nm laser using 500 ms exposure time with a final pixel size of 130 nm. For each cell, an area of 66×151 pixels covering half of the nucleus was bleached with a 561 nm laser which was moved with a dwell time of of 50 µs over the bleaching area and images were acquired every 1.51 s. For analysis, the intensity of the spot and the nucleus were manually measured in Fiji for each timepoint and the background was subtracted from the obtained values. Visible spot intensities were normalized by subtracting the respective nucleus intensity and dividing by pre-bleach intensity of the spot. For mCherry controls, the measured mCherry intensities at the visible GFP spots were divided by pre-bleach intensity of the spot. Images of cells with visible drift were discarded.

Intensity measurement of cellular GFP-HP1β after cycloheximide treatment

We previously generated GFP-HP1β knocked in mESCs (47). We seeded 2×10^4 cells or 2×10^5 cells into 96-well or on the coverslip in a 6-well plate and transfected 2 µg of mCherry or Ch-2UBA with Lipofectamine 3000 after the cells attached to the culture surface. 16 h after transfection, 100 µg/ml of cycloheximide (CHX) (Sigma, #66819) were supplemented into the culture medium. 3 h after CHX treatment, cells were fixed and permeabilized with PBS containing 0.5% Triton X-100 for 5 min at RT. Then, cells were incubated in a solution of DAPI (4',6-diamidino-2-phenylindole, 400 ng/ml in PBS) for 10 min at RT. After washing three times with PBST (PBS with 0.02% Tween), cells on coverslips were mounted with Vectashield antifade mounting medium (Vector Laboratories) and sealed with clear fingernail polish on glass slides. Cells in 96-well plates

with 100 µl of PBS were ready for image collection with an Operetta high-content imaging system.

For data analysis, the GFP-HP1β intensities in mCherry positive cells (stronger than 70 a.u.) were normalized to the mean GFP intensities of cells at the 0 h of CHX treatment. The normalized GFP-HP1β intensities were plotted with a web-tool for generation of box plots (http://shiny.chemgrid.org/boxplotr/). Unpaired *t*-test analyses were performed and *P*-values are indicated in the Figures.

ubiF3H and ubiF3Hc assays

The ubiF3H and ubiF3Hc assays were performed as described previously (32). In brief, mESC or BHK cells containing multiple lac operator repeats were transiently transfected on coverslips or 96-plates. The cell preparation for imaging were described as above.

The ubiF3H assays (Figure 2B and C) were done on coverslips in a six-well plate with 2×10^5 cells. The GFP fusion, GBP-lacI and Ch-2UBA plasmids were transiently co-expressed in a ratio of 1:1:2 (in total 2.5 µg of DNA). Cell images were collected using a Nikon TiE microscope equipped with a Yokogawa CSU-W1 spinning-disk confocal unit (50 µm pinhole size), an Andor Borealis illumination unit, Andor ALC600 laser beam combiner (405 nm/488 nm/561 nm/640 nm), Andor IXON 888 Ultra EMCCD camera and a Nikon $100\times/1.45$ NA oil immersion objective or a Leica TCS SP5 confocal microscope equipped with Plan Apo $63\times/1.4$ NA oil immersion objective and lasers with excitation lines 405, 488, 594 and 633 nm for representative images, or with an Operetta high-content imaging system for quantification. For Figure 2D, 2×10^5 of *Uhrf1* down BHK cells were seeded on coverslips and transiently co-transfected the components of the ubiF3H with 5 nM of siRNA against *Uhrf1*. 16 h after transfection, cells were fixed and sample slides prepared. Images were acquired automatically with an Operetta high-content imaging system.

For data analysis of Figure 2B, GFP and mCherry intensities at *lacO* spots were manually measured by ImageJ and the ratios were calculated for each cell: $(\text{mCherry}_{\text{Spot}} - \text{mCherry}_{\text{background}})/(\text{GFP}_{\text{Spot}} - \text{GFP}_{\text{background}})$ in order to account for different expression levels. The intensities of mCherry and GFP surrounding the spots were measured as the intensities of background. For data analyses of Figure 2D and F, cell images were analyzed with the Harmony analysis software (PerkinElmer). The cells with mCherry intensities less than 100 a.u. for Figure 2D and more than 500 a.u. for Figure 2F were filtered out. The mCherry intensities at lacO spots were normalized to the mean intensities of p53-GFP at lacO spots and plotted with a web-tool for generation of box plots (http://shiny.chemgrid.org/boxplotr/).

To test the ubiF3Hc assay (Figure 5B, C, D and 7A), all assay components including two half of YFP fusions, GBP-lacI or GBP-Lamin were transiently co-expressed in a ratio of 1:1:1:1. To improve the ubiF3Hc system, the YC fusions were stably expressed in BHK or mESCs. Then, other components including 2UBA-YN, GBP-lacI/GBP-Lamin and mCherry were transiently co-expressed in a ratio of 1:1:1 (Figure 4C, D, 6B, C and 7D). Cell images were collected using a Leica TCS SP5 confocal microscope or with an Op-

eretta high-content imaging system for quantification or a Nikon TiE microscope.

High-throughput microscopy and image analysis

The high-throughput microscopy was conducted as previously with minor differences (32). Simply, For Figure 7A, 2×10^4 BHK cells plated onto 96-well plates (Greiner Bio-One) were transiently transfected with the plasmids coding for YC-p53, 2UBA-YN, GBP-lacI and mCherry in a ratio of 1:1:1:1 (in total, 150 ng of DNA). Before transfection, the medium was supplemented with 10 μM of Nutlin-3 or DMSO (control). After 16 hours, cells were fixed with 3% formaldehyde and DNA counterstained with DAPI. After cell fixation, images were acquired automatically with an Operetta high-content imaging system at the wide-field mode using a 40× air objective (PerkinElmer). DAPI, YFP and mCherry fluorescent fusion proteins were excited, and the emissions were recorded with standard filter sets.

The images were then analyzed with the Harmony analysis software (PerkinElmer). Briefly, images were first segmented by intensity and area size according to the DAPI fluorescence using the top-hat method to define the cell nucleus area. The cell population with mCherry signals was considered as transfected cells and chosen for analysis. Then the *lacO* foci were recognized by their intensity in the YFP channel within the nuclear area of cells with mCherry signals. In these cells, the mean intensities of the YFP channel at the *lacO* were recorded, and the ratio of YFP mean intensity at the *lacO* spot to the mean intensity mCherry of the whole nucleus ($\text{YFP}_{Spot}/\text{mCherry}_{Nucleus}$) were calculated in order to account for different expression levels.

For Figure 4C and D, 2×10^4 BHK cells stably expressing YC-HP1β wt and YC-HP1β^{delC} were plated into both 96-well and 6-well plates. 2 h after plating, different combinations of assay elements were transiently transfected. The cell preparation, image acquisition and analyses are described as above.

For screening inhibitors (Figure 7C and D), different small compounds (see details in Supplementary Table S1) were prepared in a 96-well plate with the inhibitor concentration of 1 mM in DMSO. 2×10^4 BHK cells stably expressing YC-HP1β wt were plated into 96-well plates. After the cells attached to the surface, 2UBA-YN, GBP-lacI and mCherry plasmids were transfected in a ratio of 1:1:1 (in total, 150 ng of DNA). 1 hour after transfection, the compounds were added to the medium. 16 h after transfection, cells were fixed and stained with DAPI. Image acquisition and analyses are described as above.

The images from Supplementary Figure S13D were first segmented by intensity and area size according to the DAPI fluorescence using the top-hat method to define the cell nucleus area. The cell population with mCherry signals was considered as transfected cells and chosen for analysis. Then the MaSat foci were recognized by their intensity in the 488 nm channel within the nuclear area of cells with mCherry signals. In these cells, the mean intensities of the 488 nm channel at the MaSat sites and nucleus were recorded, and the YFP intensities at MaSat sites were calculated with Eq. ($\text{YFP}_{Ub} = \text{YFP}_{MaSat} - \text{YFP}_{nucleus}$).

All experiments above were repeated at least two times.

Monitoring the ubiquitination of HP1β along the cell cycle

mESCs stably expressing YC-HP1β were seeded in 2-well μslides (ibidi GmbH) coated with geltrex (Gibco, A1569601) and were transfected with plasmids coding for 2UBA-YN, GBP-Lamin and RFP-PCNA in a ratio of 2:2:1. 16 h after transfection cells were imaged with a spinning disc confocal microscope (Eclipse Ti, Nikon) equipped for live cell culture (with heating and humidified CO2 supply) as described above. YFP and RFP were excited with 488 nm and 561 nm lasers, respectively, and cells were imaged every 30 min.

For image analysis, the nuclear envelope (for YFP quantification) was segmented manually and the fluorescence intensities measured with ImageJ. The mean gray values were subtracted from the background. RFP-PCNA indicated the progression of the cell cycle and was used to align different cells for quantification. The mean gray values in the segmented area of cells at each time point were plotted.

Co-immunoprecipitation (Co-IP)

GFP and RFP-fusion pulldowns using the GFP- and RFP-Trap (ChromoTek) were performed as described (33). For detection of ubiquitinated proteins by immunoprecipitation, cells were lysed in buffer containing 150 mM KCl, 50 mM Tris–HCl (pH 7.4), 5 mM $MgCl_2$, 1% Triton X-100, 5% glycerol, 2 mM phenylmethylsulphonyl fluoride and 2 mM 2-mercaptoethanol and 5 mM NEM. After brief sonication, cell lysates were cleared by centrifugation at 4°C for 10 min. Supernatants were incubated with the GFP-Trap beads for 2 h at 4°C under gentle rotation. The beads were then washed three times with lysis buffer and resuspended in SDS-PAGE sample buffer. The anti-HA mouse monoclonal antibody 12CA5 was used for detection of ubiquitinated proteins.

In vitro ubiquitination assay

The *in vitro* ubiquitination assay was performed as previously described with minor modifications (48). His-tagged human UHRF1 was purified using Ni-NTA sepharose resin (Qiagen). Recombinant E1 (His-UBE1), E2 (GST-UbcH5b) and HA-Ub were purchased (Boston Biochem). GFP-HP1β from transfected HEK293T cells was immunoprecipitated with the GFP-Trap and incubated at 37°C for 60 min with the complete ubiquitin reaction system consisting of reaction buffer (25 mM Tris–HCl pH 7.6, 5 mM $MgCl_2$, 100 mM NaCl, 1 μM DTT, 2 mM ATP), 200 ng of E1, 200 ng of E2, 500 ng of UHRF1 and 3 μg of HA-Ub. After washing with a wash buffer (20 mM Tris–HCl pH 7.6, 150 mM NaCl and 0.5 mM EDTA), ubiquitination of HP1β was detected using an anti-Ubiquitin antibody (Santa Cruz Biotechnology).

In vivo ubiquitination assay

For detection of ubiquitinated HP1 proteins by immunoprecipitation, HEK293T cells transiently co-transfected with GFP tagged HP1 proteins with HA tagged ubiquitin (HA-Ub) were lysed in buffer containing 150 mM KCl, 50 mM Tris–HCl (pH7.4), 5mM MgCl2, 1% Triton X-100,

5% glycerol, 2 mM phenylmethylsulfonyl fluoride and 2 mM mercaptoethanol, 0.5 U/μl of benzonase and 5 mM N-Ethylmaleimide (NEM). After 30 min incubation, cell lysates were cleared by centrifugation at 4°C for 10 min. GFP-HP1β signals in supernatants were measured using a TECAN Infinite M1000 system. Then, supernatants having equal amounts of GFP-HP1β were incubated with GFP-trap beads for 2 h at 4°C with gentle rotation. The beads were then washed three times with lysis buffer and resuspended in SDS PAGE sample buffer. The anti-HA mouse monoclonal 12CA5 antibody was used for detection of ubiquitinated proteins.

For 5-aza-dC (Sigma, A3656) treatment, 1 h after transfection, 12 μM of 5-aza-dC was added into the culture medium and incubated overnight. Detection of ubiquitinated HP1β by immunoprecipitation was performed as described above. A polyclonal HP1β antibody was used for detection of GFP-HP1β.

To compare the ubiquitination levels of p53-GFP upon the Nutlin-3 treatment, the intensities of ubiquitinated p53-GFP (band: ∼80 kD) in HA blots and p53-GFP in ponceau staining blots were measured by ImageJ. The ratios were calculated for each condition: (Intensities$_{p53\text{-}GFP\text{-}Ub}$ – background)/(Intensitis$_{p53\text{-}GFP}$ -background) in order to account for different loading levels. The intensities of ubiquitinated p53-GFP and p53-GFP surrounding the bands were measured as the intensities of background.

Western blots

Following separation on SDS–PAGE, samples were transferred onto a nitrocellulose membrane and incubated with antibodies. Blots were developed with the Pierce ECL western blotting substrate (Thermo Scientific) and scanned by the Amersham™ Imager 600 system.

All antibodies used are listed in Supplementary Table S1.

siRNA knockdown, RNA Isolation and quantitative RT-PCR

100,000 BHK cells were plated into a 6-well plate and transfected with 5 nM of siRNA pool (siTOOL) against *Uhrf1* or *Usp7* by Lipofectamine 3000 (Invitrogen). After 24 or 48 hours, cells were harvested for RNA isolation or kept for further assays.

Total RNA was isolated from wt and *Uhrf1*- or *Usp7*-knockdown BHK cells using the nucleospin triprep kit from Macherey-Nagel. 500 ng of total RNA was reverse transcribed with a high-capacity cDNA reverse transcription kit (Applied Biosystems) according to the manufacturer's instructions. Real-time PCR was conducted using LightCycler® 480 SYBR Green I Master (Roche) on a LightCycler® 480 System (Roche). PCR efficiency and primer pair specificity were examined using a standard curve of serially diluted cDNA and melting curve, respectively. After normalizing to the transcript level of *Usp7* or *Uhrf1*, data was analyzed based on the $2^{-\Delta\Delta Ct}$ method.

RESULTS

Generation of a genetically encoded ubiquitin probe

Studies of protein ubiquitination mostly rely on biochemical endpoint assays using immunoprecipitation, WB analyses and mass spectrometry. To investigate protein ubiquitination in live cells we generated a genetically encoded fluorescent probe based on a naturally occurring ubiquitin binding domain. RAD23 is a DNA repair protein that interacts with the proteasome and shows ubiquitin linkage independent binding for K48- and K63-linked polyubiquitin chains (21,49,50). We fused two ubiquitin-binding domains from RAD23 in tandem with GFP (GFP-2UBA) (Figure 1A and Supplementary Figure S1A). To test the binding and precipitation efficiency, we transiently expressed HA-tagged ubiquitin (HA-Ub) together with GFP-2UBA in HEK293T cells and analyzed the co-precipitated ubiquitinated proteins with an HA antibody. Compared with the GFP control, GFP-2UBA was efficient in the specific precipitation of ubiquitinated proteins (Figure 1B).

The RING E3 ubiquitin ligase UHRF1 (also known as Np95 or ICBP90) controls DNA methylation by recruiting the maintenance DNA methyltransferase DNMT1 to hemimethylated DNA substrates (30,51–53). To screen for UHRF1 dependent ubiquitination targets, we combined this GFP-2UBA pull down approach with quantitative mass spectrometry analysis by comparing wild-type (wt) and *Uhrf1*-deficient mESCs (Figure 1C). Briefly, wt and *Uhrf1*-deficient mESCs transfected with a GFP-2UBA expression construct were grown in 'light' or 'heavy' SILAC medium. Equal amounts of nuclear extracts from 'light' and 'heavy' mESCs were mixed and incubated with the GFP-Trap. Following incubation and washing steps, bound proteins were separated and analyzed by liquid chromatography tandem mass spectrometry (LC–MS/MS). Analysis of heavy to light ratios identified proteins that are less ubiquitinated in *Uhrf1*-deficient cells (Figure 1D), suggesting likely candidates for ubiquitination. In our further analysis, we focused on the heterochromatin proteins HP1β and HP1γ as they represent potential new links of UHRF1 and epigenetic regulation.

Visualizing the ubiquitination of specific proteins in live cells

To monitor the ubiquitination of selected POIs we combined the recombinant ubiquitin probe with our previously developed F3H assay (32) to develop a ubiquitin fluorescent-three-hybrid (ubiF3H) assay. In this assay, GFP fusion proteins are anchored at a defined subcellular structure like, e.g. the nuclear envelope or a *lac* operator (*lac*O) array inserted in the genome by GFP binding proteins (GBP) and visible as a spot of enriched GFP fluorescence in the nucleus. The ubiquitination of GFP fusion proteins was detected with a mCherry-tagged tandem UBA fusion protein that accumulates at the *lac*O spot if the immobilized GFP fusion proteins are ubiquitinated. The ubiquitin probe can detect ubiquitination changes of POI that are regulated by E3 ligases and deubiquitinases (DUBs) (Figure 2A). We selected the tandem Ch-2UBA fusion as it showed better binding to the test substrate (GFP-Ub) than the simpler Ch-UBA (Supplementary Figure S1B and C). Based on the mass spectrometry results (Figure 1D), we focused on the ubiquitination of HP1 proteins. While GFP-HP1β and GFP-HP1γ showed accumulation of Ch-2UBA at the *lac*O spot, no ubiquitination was detected for GFP-HP1α
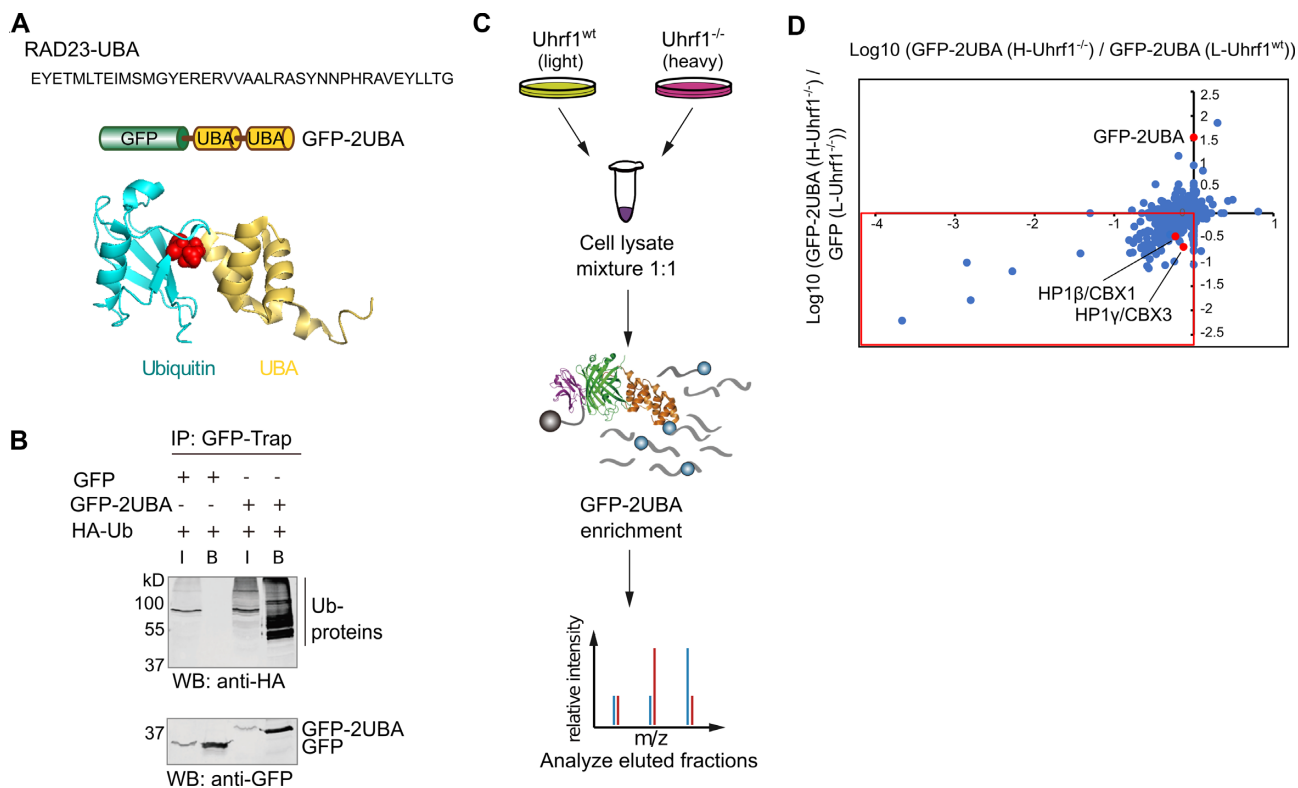
Figure 1. A ubiquitin binding domain co-precipitates with ubiquitin and detects ubiquitination in living cells. (**A**) Structure and schematic representation of the UBA fluorescent fusion protein as well as the sequence of the UBA domain used to purify ubiquitinated proteins. The structure of the UBA domain (yellow) bound to ubiquitin (cyan) is based on PDB ID code 1WR1. Residue Ile44 at the binding interface of ubiquitin is highlighted in red. (**B**) Immunoprecipitations with the GFP-Trap from HEK293T cells expressing HA-Ub and GFP-2UBA were probed with an anti-HA antibody to detect coprecipitated ubiquitinated proteins. I and B denote input and bound fractions, respectively. (**C**) Workflow for identification of UHRF1 ubiquitination targets by SILAC-MS. In this experiment, wt and *Uhrf1*-deficient mESCs were labeled with 'light' and 'heavy' SILAC medium, respectively. Equal amounts of nuclear extracts from 'light' and 'heavy' mESCs expressing GFP-2UBA were mixed for immunoprecipitation. Ubiquitinated proteins were purified with the GFP-Trap and analyzed by LC–MS/MS. (**D**) Scatter plot from heavy/light ratios of all proteins quantified in the samples indicated. HP1β and HP1γ are highlighted as potential candidates.

(Figure 2B and C). The results are in agreement with immunoprecipitation and WB analyses showing that, in contrast to GFP-HP1γ and RFP-HP1α, GFP-HP1β is strongly ubiquitinated (Supplementary Figure S2A).

To investigate the binding dynamics of Ch-2UBA in live cells, we performed fluorescence loss in photobleaching (FLIP). We found that the binding of Ch-2UBA to ubiquitinated HP1β is very transient (Supplementary Figure S3). Further, we transiently expressed mCherry or Ch-2UBA in GFP-HP1β knocked in mESCs. We measured the GFP-HP1β intensities in mCherry or Ch-2UBA positive cells and found reductions in both cells after cycloheximide (CHX) treatment (Supplementary Figure S4). Thus, the transient binding of the ubiquitin probes enables monitoring protein ubiquitination in live cells without interference with biological function.

To identify potential ubiquitination sites, we aligned the three HP1 protein sequences and found three lysine residues at the C-terminus of HP1β not present in HP1γ and HP1α (Supplementary Figure S2B). Interestingly, these three lysine residues are also part of the recognition sequence KxxxK of the ubiquitin protease USP7 (Supplementary Figure S11A) (54,55). The deletion of the last six amino acids including this KxxxK sequence (GFP-

HP1β^{delC}) caused a clear reduction in HP1β ubiquitination (Supplementary Figure S2C).

Identification of E3 ligases that ubiquitinate proteins of interest

To identify E3 ligases responsible for the ubiquitination of specific proteins we combined our live cell assay with genetic depletion or ectopic expression approaches. We focused on the ubiquitination of HP1β and investigated whether UHRF1 is the E3 ligase, as indicated by the MS screen (Figure 1D). We first performed *in vitro* ubiquitination assays, in which we immobilized GFP-HP1β on GFP-Trap beads and incubated with recombinant ubiquitin-activating enzyme (E1), ubiquitin-conjugating enzyme (E2), HA-Ub and increasing amounts of His-UHRF1. WB analysis showed clear ubiquitination of GFP-HP1β with increasing amounts of His-UHRF1 (Supplementary Figure S5A), demonstrating that UHRF1 acts as a ubiquitin E3 ligase for the modification of HP1β. We then performed ubiF3H assays in *Uhrf1*-knockdown cells and found a clear reduction of Ch-2UBA at the GFP-HP1β spot (Figure 2B, C, D and Supplementary Figure S5B), similar to DNMT1,
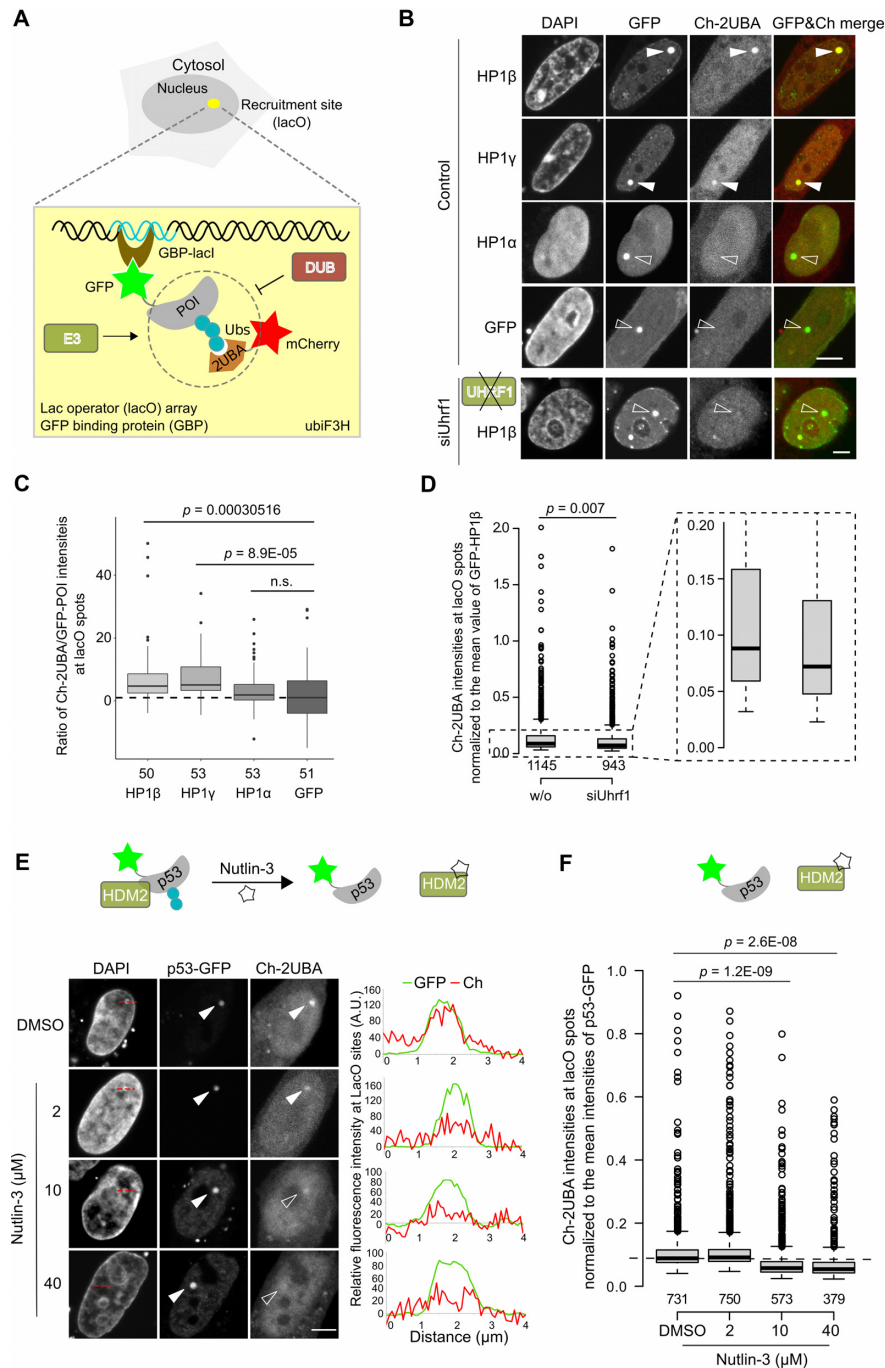
Figure 2. Visualization of the ubiquitination of specific proteins. (**A**) Schematic representation of the ubiF3H assay to monitor specific protein ubiquitination in live cells. GBP is fused with lacI that accumulates at a *lac* operator (*lacO*) array within the cell. This complex recruits to that particular spot GFP-tagged proteins of interest (GFP-POI). Ubiquitinated GFP-POI can be detected by the Ch-2UBA and visualized using fluorescent microscopy. (**B**) Ubiquitination of all three HP1 proteins was assayed by ubiF3H assays in BHK wt and compared with *Uhrf1*-knockdown cells (see Supplementary Figure S5B). The GFP-HP1 fusion proteins were transiently co-expressed with Ch-2UBA and GBP-lacI in BHK cells. The Ch-2UBA accumulation at *lacO* spots reflects ubiquitination of GFP fusion proteins highlighted with filled arrowheads and not detectable ubiquitination is indicated with open arrowheads. Scale bars: 5 μm. (**C, D**) Boxplots for the quantifications of (**B**). The ubiquitination of HP1 proteins in C and HP1β ubiquitination when Uhrf1 is knocked down in D. Center lines show the medians; box limits indicate the 25th and 75th percentiles as determined by R software; whiskers extend 1.5 times the interquartile range from the 25th and 75th percentiles, outliers are represented by dots. Two negative outliers are not depicted in the graph. The number of cells analyzed is indicated in the Figure. Data sets were tested for significance using a pairwise Wilcoxon rank-sum test with Bonferroni correction for C and an unpaired t-test for D. The p-values are indicated. (**E**) Representative images showing the disruption of HDM2 mediated ubiquitination of p53-GFP by Nutlin-3 at 0 (DMSO, control), 2, 10 and 40 μM. Line scans along lacO spots (red dot lines in the DAPI channel) are shown on the side. Scale bar: 5 μm. Schematic representation of the disruption of p53-GFP and HDM2 interaction by Nutlin-3 is shown above. (**F**) Box plot representations of the ubiquitination of p53-GFP in the presence of different amounts of Nutlin-3. Center lines show the medians; box limits indicate the 25th and 75th percentiles as determined by R software; whiskers extend 1.5 times the interquartile range from the 25th and 75th percentiles; outliers are represented by dots. The number of cells analyzed is indicated in the Figure. Data sets were tested for significance with an unpaired t-test and p-values are indicated.

H3 and PAF15 (Supplementary Figure S5C), the known ubiquitin substrates of UHRF1 (29,30,52,56–58).

As an additional example, we chose the tumour suppressor p53, one of the most studied proteins in cancer research. The ubiquitin E3 ligase HDM2 ubiquitinates p53 and thereby targets it for degradation (59). The cancer drug Nutlin-3 had been developed as a specific inhibitor to disrupt the p53-HDM2 interaction (60), and thereby prevent p53 ubiquitination (Figure 2E). With our Ch-2UBA probe, we clearly detected ubiquitination at the p53-GFP spot in control cells (DMSO) (Figure 2E). The accumulation of Ch-2UBA at *lacO* spots, however, significantly decreased in the presence of more than 10 μM Nutlin-3 indicating reduced ubiquitination of p53 (Figure 2E and F). Consistently, we detected reductions of p53-GFP ubiquitination upon the treatment of Nutlin-3 by *in vivo* ubiquitination assay (Supplementary Figure S6). These results show that our assay is well suited to identify E3 ligases responsible for the ubiquitination of specific proteins and to directly screen for inhibitors in live cells.

Probes discriminating K48 and K63 ubiquitin linkages

To distinguish the most abundant K48 and K63 ubiquitin linkages (Figure 3A), we fused ubiquitin interacting motifs (2UIM) from USP25 (61) and the NZF from TAK1 binding protein 2 (TAB2) (24,62) with mCherry to generate specific ubiquitin probes (Ch-2UIM and Ch-NZF) (Supplementary Figure S7A). The 2UIM specifically recognizes K48 ubiquitin linkage via binding the proximal ubiquitin with UIM2 and to the distal one with UIM1 (63), while the NZF binds the Ile44 patch of both proximal and distal ubiquitin to specifically recognize the K63 ubiquitin linkage (62) (Figure 3B, Supplementary Figure S7A).

We used these ubiquitin probes to analyze the ubiquitination of PAF15 (mono-Ub) (57,58), DNMT3A (K63-Ub) (64), p21 (K48- and K63-Ub) (65,66), Cyclin B1 (K11-Ub) (67), p53 (K48-Ub) (68) and H2A (mono- and K63-Ub) (69,70) (Figure 3C, Supplementary Figure S7B and 8). The binding preferences detected with Ch-2UIM and Ch-NZF are summarized in Figure 3C and are consistent with the mostly biochemistry-based analyses cited above. These results show that the two recombinant probes, Ch-2UIM and Ch-NZF, specifically detect K48- and K63-linked ubiquitin chains, respectively, while Ch-2UBA (Supplementary Figure S7A) shows a linkage independent binding.

Detecting protein ubiquitination in live cells with recombinant ubiquitin probes

To test the ability of ubiquitin probes to detect ubiquitination in live cells, we chose DNA damage sites which feature high levels of protein ubiquitination. We locally induced DNA damage in cultured cells stably expressing GFP-tagged proliferating cell nuclear antigen (GFP-PCNA) and ectopically expressing mCherry tagged ubiquitin probes. Repair at DNA damage sites has been shown to involve PCNA, and to elicit ubiquitination and proteasome-mediated degradation (71–73). To locally induce DNA damage, we irradiated a spot in the nucleus with a focused 405 nm laser. Using live-cell imaging, we monitored GFP-PCNA accumulation as a readout of DNA damage and

repair. Accumulation of mCherry tagged ubiquitin probes at the spot of GFP-PCNA accumulation shows that our probes can detect ubiquitination in response to DNA damage (Figure 3D, E). By combining these three recombinant probes, we further ascertained the ubiquitination dynamics during DNA repair. We found that Ch-2UIM (K48) showed the fastest association with DNA damage sites (time of 50% recruitment ($t_{1/2}$): ~17 sec) versus Ch-2UBA (K48 and K63, $t_{1/2}$: ~24 s) and Ch-NZF (K63, $t_{1/2}$: ~30 s) (Figure 3F and G). In line with previous studies (74–78), we found that K48-linked polyubiquitination mediates protein degradation and nucleosome eviction at DNA damage sites and facilitates following K63-linked ubiquitination mediated signaling repair pathways. Interestingly, Ch-2UBA and Ch-NZF exhibited stable association with damage sites over one hour, whereas Ch-2UIM dissociated from DNA damage sites after 10 min and its retention time was more variable between cells than of the other two probes (Figure 3F and G). Our observation that the stability of Ch-2UIM binding to the damaged spot was lower indicating its rapid turnover (Figure 3F and G), suggests that the K48 chain formation is short-lived, and less uniform compared to K63 (76,79) during DNA damage response.

Enhancing the detection of protein ubiquitination by fluorescence complementation

To further enhance the signal-to-noise ratio and to obtain a single-color readout, we combined this ubiF3H spot assay with a previously described split-YFP (9,80) to develop a ubiquitin fluorescence-three-hybrid complementation (ubiF3Hc) assay (Figure 4A). Briefly, the POI was tagged with the C-terminal half of YFP, whereas 2UBA was tagged with the N-terminal half of YFP. An interaction between POI and 2UBA leading to complementation of both YFP halves yields a functional fluorescent YFP protein, detectable by fluorescence microscopy. YFP shares a high similarity with GFP (Supplementary Figure S9A) and is also recognized by the GFP binding nanobody GBP (33). The crystal structure of the GFP-GBP complex shows that the interface extends over both halves of the split YFP and the GBP binds amino acids of the N- and the C-terminal half of the split YFP (34) to enhance YFP fluorescence (Figure 4B and Supplementary Figure S9B). We visualized the ubiquitination of PAF15 in local cellular sites (Supplementary Figure S9C and D). As most ubiquitinated proteins are not abundant, the reconstituted YFP proteins are captured at the *lacO* spot using GBPs to improve the signal-to-noise ratio (Figure 4A). Using the ubiF3Hc assay we confirmed the ubiquitination of HP1β (Figure 4C). To test the potential usage of ubiF3Hc assay in mapping ubiquitination sites, we stably expressed YC-HP1β wt and YC-HP1β^delC in BHK cells (Supplementary Figure S10). By transiently expressing the other components, we found significant reduction of HP1β ubiquitination with the HP1β^delC mutant (Figure 4C and D) that is in consistency with our biochemical data (Supplementary Figure S2C). Comparison of the ubiF3H assay in Figure 2B shows that the signal-to-noise ratios are much higher in ubiF3Hc than ubiF3H.

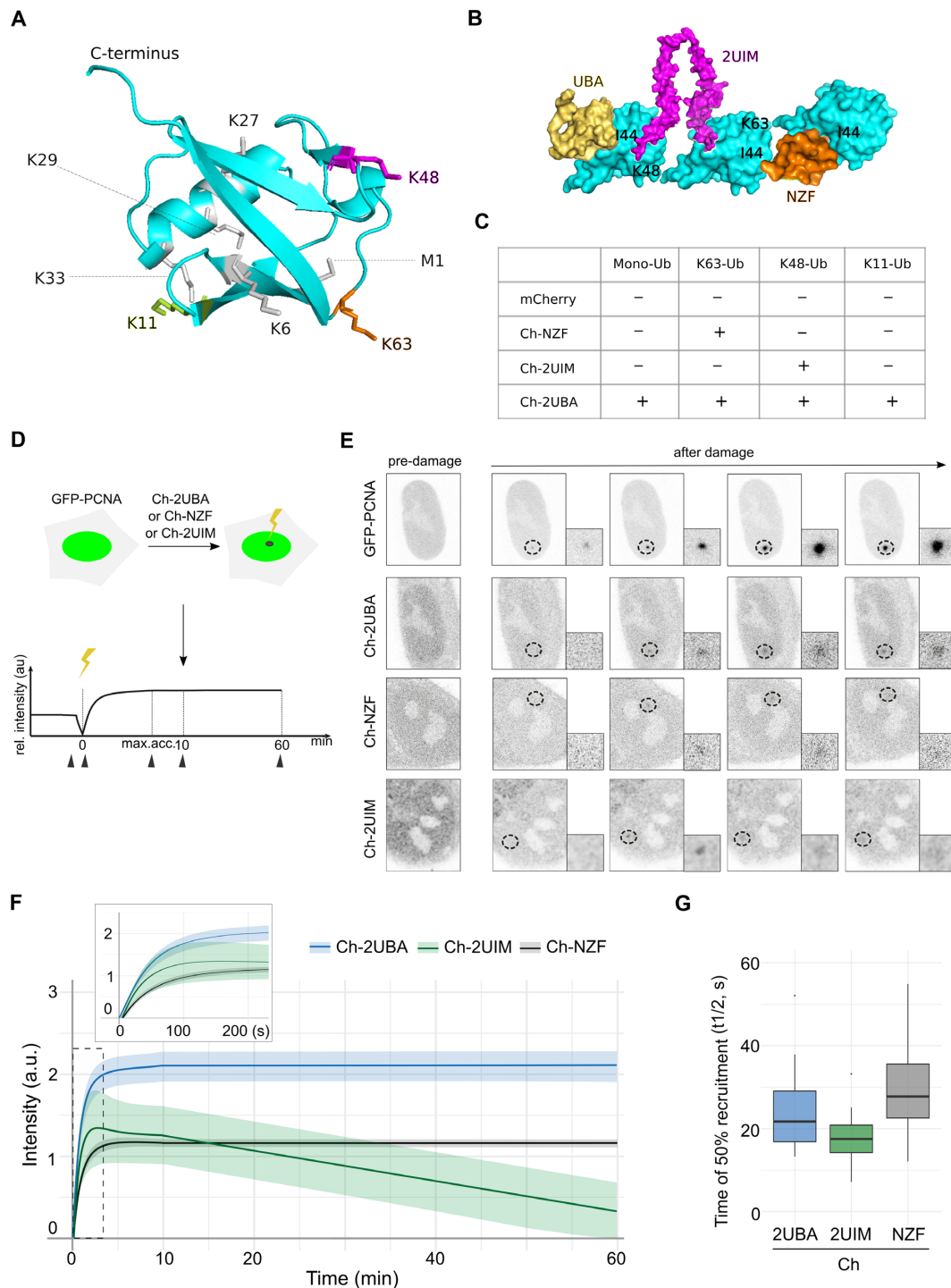We next investigated whether USP7 is the DUB for the deubiquitination of HP1β, as its recognition sequence

Figure 3. Discriminating K48 and K63 ubiquitin linkages in live cells. (**A**) The structure of ubiquitin (cyan, PDB ID code 1UBQ) and its seven lysine residues for the linkage formation. All seven lysine residues (K6, K11, K27, K29, K33, K48, and K63) and the N-terminal amino group (M1) residing on different sides of the molecule are labeled. (**B**) Schematic representation of K48 and K63 ubiquitin linkages recognized by UBA, 2UIM and NZF (see details in Supplementary Figure S7A). (**C**) Summary of the binding preference based on ubiquitination detections of GFP tagged PAF15, DNMT3A, p21, Cyclin B1, p53 and H2A using different ubiquitin probes. Representative images are shown in Supplementary Figure S7B. The binding preference of ubiquitin probes is summarized according to the quantifications shown in Supplementary Figure S8. (**D**) Schematic representation of ubiquitin probes used to monitor protein ubiquitination in live cells at DNA damage sites. (**E**) Representative images corresponding to the time points indicated in (D) with black arrowheads. DNA damage was locally induced by microirradiation (black dotted circle) and zoomed images are shown. The Ch-2UIM image was processed for better representation of the signal: raw image was multiplied by itself, then processed with ROF denoise filter (theta 100) and Gaussian filter (sigma 1.5). (**F**) Ubiquitin probes recruitment curves displayed as mean ± SEM for two or three independent experiments after DNA damage. For each experimental condition at least 25 cells were used. The dotted region is shown as a magnified insert to better illustrate the recruitments of ubiquitin probes within 200 seconds after DNA damage. (**G**) Times of 50% recruitment of ubiquitin probes at DNA damage sites represented as boxplots. Middle line depicts the median value among the cell population.
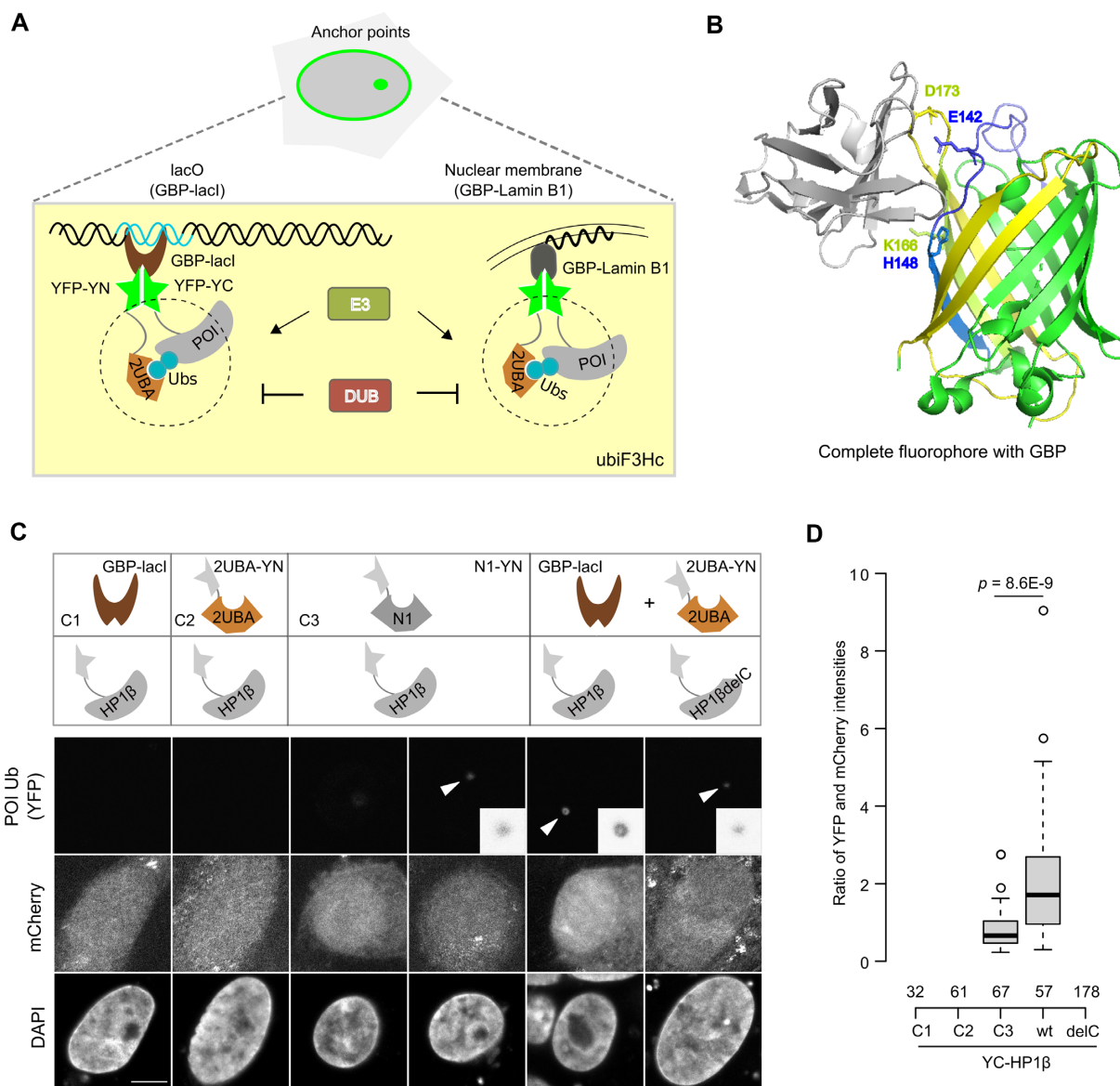
Figure 4. Visualization of the ubiquitination of specific proteins by ubiF3Hc. (**A**) Schematic representation of a fluorescent protein complementation assay using split YFP fusions, to probe interactions between POIs, fused to the C-terminal half of YFP (YC), and 2UBA, fused to the N-terminal half of YFP (YN). The reconstituted YFP was trapped at the *lacO* array or nuclear membrane by GBP-lacI and GBP-Lamin B1 fusion proteins, respectively. (**B**) The active reconstituted GFP with GBP protein (PDB ID code 3K1K) is shown and the major amino acids in the binding surface from GFP are highlighted. The GBP protein is labeled in gray. (**C**) Representative images of HP1β wt and HP1β^delC ubiquitination with the ubiF3Hc assay in BHK cells. YC-HP1β wt or YC-HP1β^delC was stably expressed in BHK cells and other components of the ubiF3Hc assay were transiently expressed. The expression of mCherry was used to identify transfected cells. A nanobody fused to the N-terminal half of YFP (YN-N1) and different combinations of those elements were used as negative controls named C1, C2 and C3. The YFP spots were highlighted with white arrows and their zoomed in images show on the sides. Scale bar: 5 μm. (**D**) Box plot representations of intensity ratios of YFP and mCherry intensities at *lacO* spots. Center lines show the medians; box limits indicate the 25th and 75th percentiles as determined by R software; whiskers extend 1.5 times the interquartile range from the 25th and 75th percentiles; outliers are represented by dots. The numbers of cells analyzed are indicated in the plot. There are no spots (YFP, ubiquitinated HP1βdelC) identified and thus no box is shown for HP1βdelC. Data sets were tested for significance with an unpaired *t*-test and *P*-values are indicated.

KxxxK (54,55) is found in HP1β (Supplementary Figure S11A). We observed a significant increase of HP1β ubiquitination in *Usp7*-knockdown cells (Supplementary Figure S11B–D) similar to the positive control H3 (81). Consistently, biochemical analyses showed that GFP-HP1β polyubiquitination was reduced to undetectable levels by co-expression of Ch-USP7, but not the catalytically inactive point mutant Ch-USP7^C224S (Supplementary Figure S11E).

Monitoring protein ubiquitination along the cell cycle

The ubiF3Hc approach not only improves the signal-to-noise ratio but also frees one color channel for additional readouts to investigate correlations with other cellular processes like, e.g. cell cycle progression by co-expression of RFP-PCNA as S phase marker (82). While the *lacO* array serves as an efficient anchor point for F3H assays and yields easy to analyze spot signals, it also limits the usage to cells

genetically engineered to carry this array. In this regard, besides this *lac*O, also other cellular structures like the nuclear envelope, actin filaments or centrosomes may be used as anchor points for the F3H assays, which allows an easy transfer to other subcellular environments, cell systems and species (32) (Figure 4A).

Thus, we applied the ubiF3Hc assay in mESCs using the nuclear envelope as an anchor point to investigate the ubiquitination of PAF15 and H3 during the cell cycle. Recently, we reported that UHRF1 ubiquitinates PAF15 and H3 recruiting DNMT1 for the maintenance of DNA methylation after DNA replication (52) (Figure 5A). We compared the ubiquitination timing of PAF15 and H3 during the cell cycle by using the ubiF3Hc assay. We found that PAF15 is predominantly ubiquitinated in the early S phase, while H3 is modified in both early- and middle-S phases (Figure 5B and C). A closer look shows H3 ubiquitination signals throughout the nucleus that seem to accumulate at the rim over time reflecting YFP capture by GBP-Lamin B1 (Supplementary Figure S12). This result is consistent with our finding that PAF15 is preferentially involved in the methylation of early replicating DNA (58). We did not detect ubiquitination of PAF15 and H3 in late S phase.

With the same assay, we found that the ubiquitination of HP1β predominantly occurs in S phase (Figure 5D and E). In parallel, we investigated whether HP1β is subjected to cell cycle dependent regulation by biochemical analyses. In this assay, cells arrested in late G1 phase by mimosine were tested for HP1β abundance at different times after release into the cell cycle. Cell cycle progression was monitored by flow cytometry (Figure 5F). Consistently, time course analysis of cells released from mimosine G1 arrest showed that HP1β levels decreased in S phase (Figure 5F), which is consistent with the observed ubiquitination of HP1β (mostly) in S phase. Furthermore, we detected an increase of HP1β level in *Uhrf1*-deficient cells (Supplementary Figure S13A). These results suggest that UHRF1 ubiquitinates HP1β in S-phase and targets it for degradation.

Thus, our results show that the ubiF3Hc assay can complement and extend biochemical approaches and provide insights into cell cycle dependent changes in protein ubiquitination.

To test the application of ubiF3Hc in monitoring the ubiquitination of specific proteins in live cells, we stably expressed the HP1β fused with the C-terminal half of YFP and transiently expressed the other components. The ubiquitinated HP1β (YFP-HP1β Ub) was recruited to the nuclear envelope (Figure 6A and Supplementary Figure S13B). With live cell microscopy, we monitored the ubiquitination of HP1β during cell cycle and consistently observed its ubiquitination in S-phase (Figure 6B and C).

Identification of targets and inhibitors of ubiquitination in live cells

As the ubiF3Hc assay shows a high signal-to-noise ratio, we next sought to examine whether it is applicable for high-throughput screening in drug discovery. We tested this assay in 96-well plates to automatically visualize and analyze HP1β ubiquitination. In line with the result shown in Figure 2B and 4C, we observed clear reconstituted YFP

signals at *lacO* spots in two independent replicates showing HP1β ubiquitination and demonstrating the robustness of the ubiF3Hc assay (Supplementary Figure S13C). We further recruited ubiquitinated proteins to major satellites (MaSat) that allows the application of ubiF3Hc in any mouse cell types.

To test the potential of this system for identification of E3 ligases, we stably expressed the YC-HP1β and YC-PAF15, the ubiquitination targets of UHRF1, in mESCs (Supplementary Figure S13B). We then analyzed their ubiquitination level after knock down of *Uhrf1*. As a control, we analyzed the ubiquitination of PAF15 in UHRF1 ubiquitination defective cells (UHRF1 H730A) (83). In line with the result shown in Supplementary Figure S5C, we detected significant reductions of PAF15 ubiquitination in both UHRF1 H730A and *Uhrf1* knocked down cells (Supplementary Figure S13D). Likewise, we observed a reduction of HP1β ubiquitination in *Uhrf1* knocked down cells (Supplementary Figure S13D) that is in line with our MS result (Figure 1D).

To investigate the potential of this ubiF3Hc assay for the identification of specific inhibitors, we chose the well-known tumor suppressor p53 which is ubiquitinated by HDM2 and thus marked for degradation (59). To restore and boost p53 tumor suppressor activity in cancer therapy, small molecules like Nutlin-3 have been developed to inhibit the ubiquitination by HDM2 (60). We expressed the components of the ubiF3Hc assay for detection of p53 ubiquitination and clearly observed reconstituted YFP signals at *lacO* spots in consistency with Figure 2E and F. We then incubated the cells with 10 μM Nutlin-3 to test the potential of this assay for the identification of specific inhibitors. The reconstituted YFP signals at *lacO* spots significantly decreased indicating reduced ubiquitination of p53 (Figure 7A and B). These results show that our ubiF3Hc assay is suited to detect the ubiquitination of the tumor suppressor p53 and to identify specific inhibitors like Nutlin-3.

We next expanded it to a small-scale screen for small compounds and tested their ability to regulate HP1β ubiquitination. We tested eight inhibitors including TBB, an inhibitor specific for casein kinase II (CK2), GNE-0640, an inhibitor for USP7, CHIR, a potent glycogen synthase kinase (GSK) 3 inhibitor, PD, an inhibitor for MAPK/ERK, PP1, an ATP-competitive inhibitor of mutant over wild-type kinases. We used YC-HP1β BHK cells and transiently expressed other components of the ubiF3Hc assay to measure the ubiquitination of HP1β in the presence of different inhibitors from 3 to 12 μM (Figure 7C, D and Supplementary Figure S14A). We found that the level of HP1β ubiquitination did not change at the concentration of 3 μM but showed a significant reduction at the concentration of 12 μM for TBB. 5-aza-dC but not Nutlin-3 increased the ubiquitination of HP1β and this was dose-dependent (from 3 to 12 μM) (Figure 7D and Supplementary Figure S14A). Notably, with increasing concentration of GNE-6640, mCherry positive cells identified were much less than with the control (DMSO), which may be due to toxic effects on the cells or negative influence on the transfection at the concentration range used (3 to 12 μM). Thus, we tested GNE-6640 at the concentration of 0.6 μM (around its IC50) and found that inhibition of
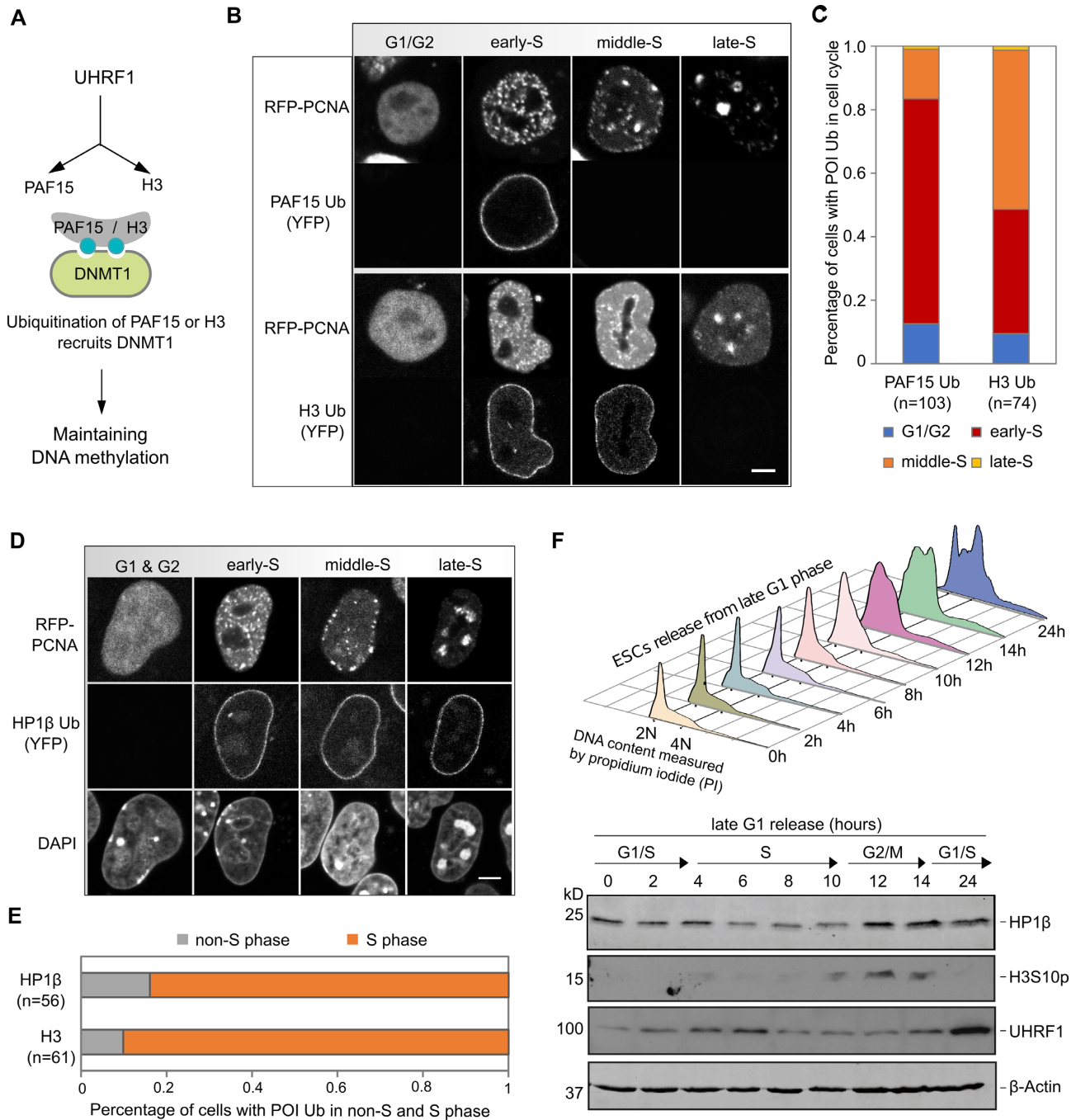
Figure 5. Visualization of cell cycle dependent ubiquitination. (**A**) Illustration of two distinct modes of DNMT1 recruitment after DNA replication for the maintenance of DNA methylation. (**B**) Representative images of cell cycle dependent ubiquitination of PAF15 and H3. Scale bar: 5 µm. (**C**) Percentage of cells with PAF15 and H3 ubiquitination during the cell cycle. The numbers of cells analyzed (n) are indicated. (**D**) Representative images of cell cycle dependent ubiquitination of HP1β in mESCs using the nuclear envelope as an anchor point and RFP-PCNA as a cell cycle indicator. Scale bar: 5 µm. (**E**) Percentage of cells with H3 and HP1β ubiquitination in non-S and S phase. The numbers of cells analyzed (n) are indicated. (**F**) HP1β and UHRF1 levels in synchronized mESCs released from the late G1 phase were detected by WB. The H3S10p blot was used to highlight the G2 phase, and the actin blot was shown as loading control. Cell cycle profiles of synchronized mESCs are shown above for each time point after release from the late G1 phase.
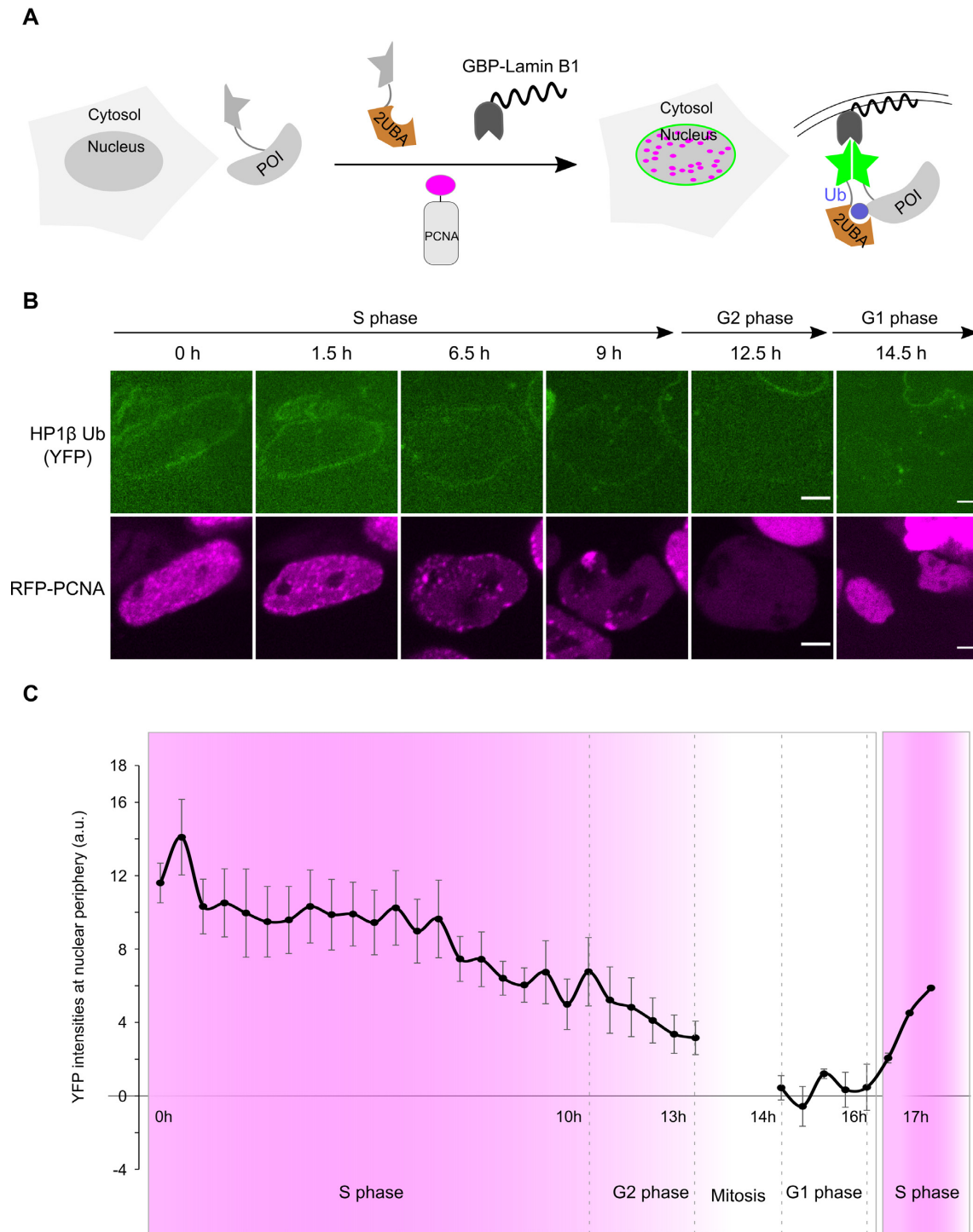
Figure 6. Monitoring the ubiquitination of HP1β in live cells during cell cycle. (**A**) Schematic outline of the protein ubiquitination monitoring strategy. POI fused with the C-terminal half of YFP was stably expressed in mESCs and other components were transiently expressed to recruit the ubiquitinated protein to nuclear envelope. (**B**) Live cell series of mESCs stably expressing YC-HP1β and transiently co-expressing components shown in (A). Scale bars: 5 μm. (**C**) Time lapse quantification of the YFP (HP1β-Ub) intensities at the nuclear lamina. Five individual cells were aligned and the mean and the SEM of the YFP intensities were shown. The images of cells at mitosis states are excluded from the quantification. The last two time points were derived from one single cell.

the ubiquitin-specific protease USP7 by GNE-6640 leads to the upregulation of HP1β ubiquitination (Supplementary Figure S14B). To confirm the screening result, we performed an *in vivo* ubiquitination assay and consistently found that 5-aza-dC treatment induced the ubiquitination of HP1β (Figure 7E).

Thus, the ubiF3H assay is a robust tool for studying protein ubiquitination in live cells. We could use ubiF3H assays to monitor the ubiquiting of specific proteins in live cells, to identify E3 ubiquitin ligases and proteases, to map the ubiquitination sites and to discriminate different ubiquitin linkages. The ubiF3Hc assay is suitable for studying temporal protein ubiquitination in live cells and high-throughput screens with small molecule or siRNA libraries.

Importantly, the ubiF3Hc assay is suitable for studying temporal changes in protein ubiquitination and screens with small molecules or siRNAs in live cells.

DISCUSSION

Protein regulatory networks are largely governed by posttranslational modifications and proteasome-mediated degradation, whereby ubiquitination plays a central role. As protein ubiquitination occurs in different configurations and functions, the key to a comprehensive understanding of this dynamic and multifaceted posttranslational modification is the identification of targets with their respective ligases and proteases along with the timing and linkage of this modification. Targets are typically identified by immunoprecipitation with antibodies against the diGly motive remaining after digestion of ubiquitinated proteins as we previously used to identify UHRF1 targets (57). Here, we co-expressed a GFP-2UBA fusion and enriched ubiquitinated proteins with our nanobody against GFP (GBP) for quantitative MS analysis. We screened UHRF1 dependent ubiquitination targets by comparing *Uhrf1*-deficient versus wt mESCs and identified the heterochromatin protein HP1β as a novel substrate which had not been picked up in our prior study using an antibody against diGly (57). In general, however, the enrichment with the co-expressed GFP-2UBA was less efficient and low abundant ubiquitinated proteins, like PAF15 (57) were missed. While there are some reports of HP1 ubiquitination (84) the modification of HP1β by UHRF1 had been missed so far.

The expression of GFP-2UBA allows the detection of ubiquitinated proteins in live cells in general but cannot distinguish which proteins are modified. To detect ubiquitination of specific proteins we developed the ubiF3H assay and expressed GFP fusions with POIs and immobilized them at distinct subcellular structures with the GBP. We used cell lines with a genomic *lacO* array as anchor points to obtain easy to discern spot signals for automated image analysis. To be more flexible and independent from these cell lines, also endogenous structures, like the nuclear lamina, major satellite DNA repeats, actin filaments or centrosomes, may be used as anchor points as previously demonstrated for protein interaction assays (32). Clearly, the GBP-mediated capture of GFP fusion proteins at a distinct spot also improves the signal-to-noise ratio and the intracellular dynamics seems to be sufficient so that even interactions between mitochondrial proteins could be monitored at nuclear *lacO*

spots with the original F2H assay (85). Also, for convenience we mostly relied on transient transfections but for studies at physiological expression levels, endogenous genes may be tagged as described (86). This simple ubiF3H assay was not designed for absolute quantification but provides a rapid display of the ubiquitination status of POIs and allows to monitor relative changes in the ubiquitination signal in response to defined manipulations. Thus, we could identify UHRF1 dependent ubiquitination of HP1β and identify the protease USP7 as potential antagonist of this PTM (Figs. 2B, Supplementary Figure S11 and S14). The UBA domain detects as far as we know all ubiquityl residues and is therefore ideally suited for primary screens with the ubiF3H assay. But as most information of this PTM is encoded in the linkage (2), i.e. which lysine residues are used for conjugation, we employed more specialized domains for further discrimination. To expand the scope of the ubiF3H assay, we chose the naturally occurring domains 2UIM and NZF that specifically bind K48 and K63 linked ubiquitin chains (61–63). The comparative use of these three ubiquitin binding domains in the ubiF3H assay makes it possible to discern the most prominent ubiquitin chains in live cells. The ubiF3H assay could be further expanded to identify additional types of ubiquitin chains by using natural or artificial binders like specific affimers that were developed for recognition of K6 and K11/K33 ubiquitin linkages (87).

The application of fluorescent ubiquitin binders *per se* is limited to monitoring changes in ubiquitination at distinct cellular structures or local processes. FLIP experiments (Supplementary Figure S3) suggest that the binding of ubiquitin probes is transient and will not interfere with biological functions *in vivo*. Thus, we detected an increase in ubiquitin at focal sites of DNA damage (Figure 3E) reflecting the known role of ubiquitination in e.g. DNA double-strand repair (88). The comparison of three ubiquitin chain specific probes showed a faster recruitment of 2UIM at DNA damage sites (Figure 3F and G). This early K48-ubiquitination event at the DNA damage spots is supported by previous publications highlighting, for example, RNF8-mediated K48-linked Ku80 removal (76), RNF8-mediated K48-linked VCP/p97 and 53BP1 recruitment (77,78), and L3MBTL1 degradation (74). All of these processes happen relatively early after the damaging event and contribute to the formation and stability of repair foci. Some studies have reported the rapid turnover of the K48-linked polyubiquitin chains (76,79), which has hindered the study of the K48-linked polyubiquitin chains' contribution to DNA damage signaling. On the other hand, the long retention times of Ch-2UBA and Ch-NZF can be explained by K63 polyubiquitin chains' importance at later DNA damage signaling steps, including the repair pathway choice and subsequent repair (75).

To enhance the signal-to-noise ratio of the ubiF3H assay, we implemented a fluorescence complementation (FC) approach between POI and ubiquitin reader using split YFP. While this FC approach allows detection of ubiquitination in the natural subcellular environment, it may also spread the signal throughout the cell, depending on the distribution of the POI. Therefore, we co-expressed GBP-Lamin B1 to locally capture the complemented YFP fusions at the nuclear envelope. The binding of GBP is expected to enhance
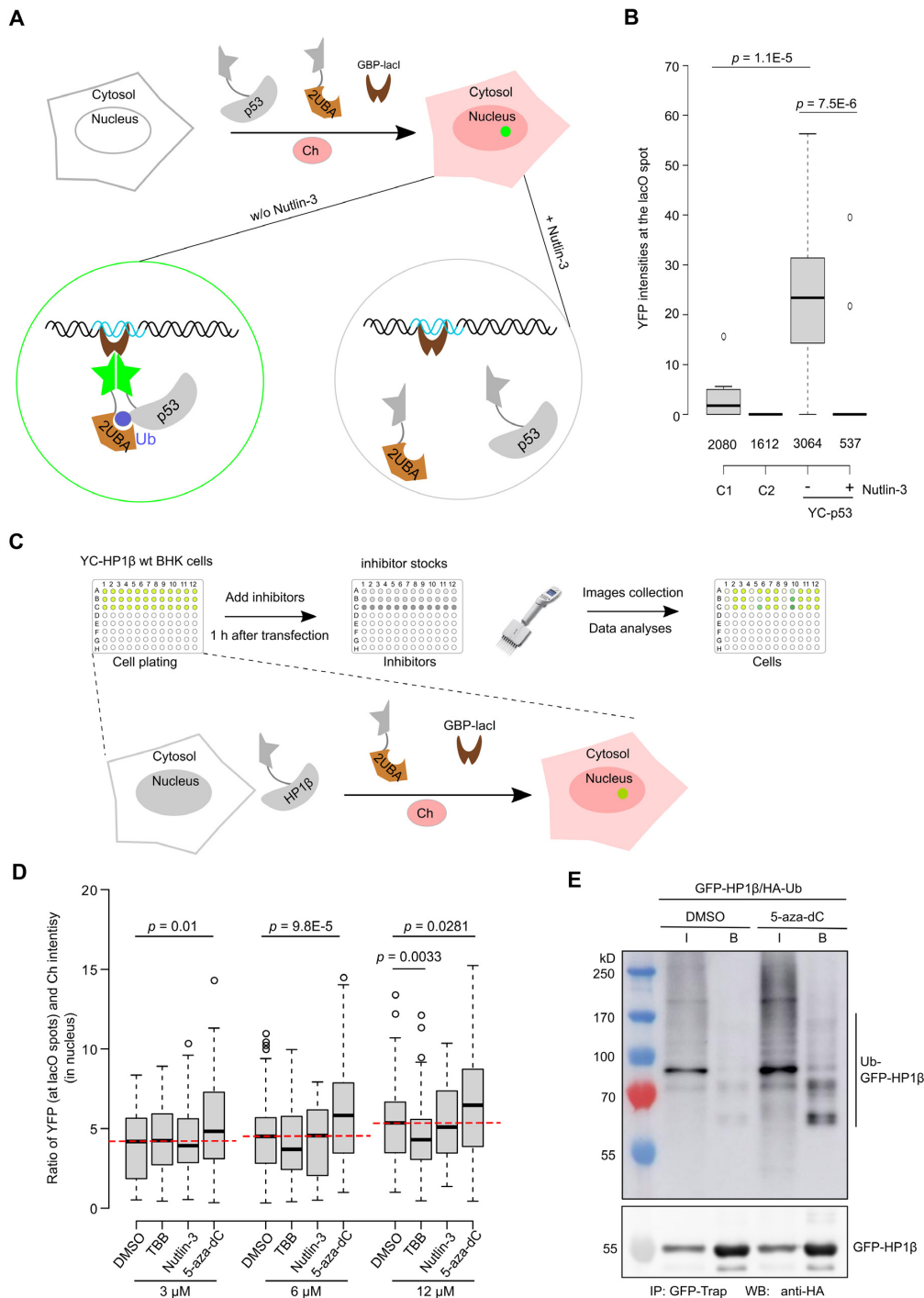
Figure 7. Identification of targets and inhibitors of ubiquitination in live cells. (**A**) Schematic outline of the detection of p53 ubiquitination in 96-well plates in the presence or absence of Nutlin-3. The components of the ubiF3Hc assay are transiently expressed in BHK cells. The expression of mCherry was used to identify transfected cells. (**B**) Box plot representations of intensity ratios of reconstituted YFP and mCherry at *lacO* spots and nucleus, respectively, for p53 ubiquitination in the absence and presence of 10 μM Nutlin-3 (right). C1 (control 1: YC-p53, N1-YN, GBP-lacI and mCherry) and C2 (control 2: YC-p53, 2UBA-YN and mCherry). Center lines show the medians; box limits indicate the 25th and 75th percentiles as determined by R software; whiskers extend 1.5 times the interquartile range from the 25th and 75th percentiles; outliers are represented by dots. The numbers of cells analyzed are indicated. Data sets were tested for significance with an unpaired t-test and *p*-values are indicated. (**C** and **D**) Screening small compounds that regulate the level of HP1β ubiquitination in a 96-well plate with ubiF3Hc assay. Working flow was shown in (C). YC-HP1β was stably expressed in BHK cells, whereas 2UBA-YN and GBP-lacI were transiently expressed in BHK cells. Box plot shows the ubiquitination levels of HP1β upon the treatment of TBB, Nutlin-3 and 5-aza-dC (see more in Supplementary Figure S14). Center lines show the medians; box limits indicate the 25th and 75th percentiles as determined by R software; whiskers extend 1.5 times the interquartile range from the 25th and 75th percentiles; outliers are represented by dots. Unpaired t-test was done and p-values were indicated (D). (**E**) GFP-HP1β ubiquitination is increased by treatment of 5-aza-dC. HEK293T cells were transfected with GFP-HP1β and HA-Ub in the presence of DMSO or 5-aza-dC. Immunoprecipitation was performed with GFP-trap and bound fractions were detected by western blot using anti-HA and HP1β antibodies.

the fluorescence of YFP as was reported for GFP (34) and to stabilize the complemented YFP as the binding interface spans both halves (Figure 4B). The local entrapment of the YFP fusions may not only improve the signal-to-noise ratio through the concentration of the signal at a distinct structure but may also slow down degradation. These features of the ubiF3Hc assay enhance the signal but complicate the quantification. Also, as FC depends on spatial proximity and steric fit, the ubiF3Hc assay may, for some POIs, require optimization of linker length and fusion site for the complementing YFP halves. In comparison with the ubiF3H assay, which essentially measures the colocalization of green and red fluorescence, the ubiF3Hc assay requires only a single-color channel (YFP) leaving another channel free for additional readouts like, e.g. the cell cycle phase, as demonstrated with RFP-PCNA (Figure 5B and D).

Previous bimolecular complementation assays relied on the covalent ligation of labeled ubiquitin (9,10). Here, we use ubiquitin binding domains, which, by the transient nature of their binding and discriminating specificity, is expected to be more dynamic, less disruptive and more informative. The comparative use of UBA, 2UIM and NZF ubiquitin binding domains in the colocalization based ubiF3H assay to discriminate between monoubiquitination versus K48 and K63 linked ubiquitin chains (Figure 3) can easily be applied to the complementation based ubiF3Hc assay. Both assays can be further expanded as more specific binding domains are either identified or artificially generated, like. e.g. the aforementioned affimers (87) making the ubiF3H assays a dynamic and powerful platform for the study of protein ubiquitination in live cells.

One important feature of the ubiF3Hc assay is the improved signal-to-noise ratio achieved by local signal enrichment at distinct subcellular structures like the nuclear envelope or the *lacO* array spot. This worked well for relatively mobile proteins like HP1β with a half recovery time ($t_{1/2}$) of 2.5 s (89) but, surprisingly, also for rather immobile proteins like core histone H3 with recovery times in the range of hours (90). It will be interesting to investigate whether the captured H3 fusion protein stems from a small mobile fraction mobilized by transcription and DNA replication or by ubiquitination itself.

The single color based ubiF3Hc assay is ideally suited to correlate the ubiquitination of specific proteins with other cellular processes like, e.g. cell cycle progression. With RFP-PCNA as a cell cycle marker we found that PAF15 and H3 are preferentially ubiquitinated in S phase (Figure 5B), which is consistent with the known function of the UHRF1 E3 ligase. A potential limitation of fluorescence based bimolecular fluorescence complementation is its reported irreversibility *in vitro* and *in vivo* (91,92). However, we monitored dynamic changes of HP1β ubiquitination during the cell cycle (Figure 6). This dynamics could be caused by reversible complementation or degradation as described before (93–95).

UHRF1 is an essential factor for the maintenance of DNA methylation after DNA replication in S phase (51,53). On the one hand, UHRF1 controls DNMT1 abundance by polyubiquitination (29,56). On the other hand, it monoubiquitinates PAF15 and histone H3, and thereby indirectly recruits DNMT1 to replication foci for the mainte-

nance of DNA methylation (30,52,58). Genetic data indicate that PAF15 ubiquitination is preferentially involved in the methylation of early replicating DNA (58) which fits well with the observed ubiquitination mostly in early S phase (Figure 5B and C). Surprisingly, no ubiquitination was detected for PAF15 and H3 in late S phase, which might point towards a third, still unknown recruiting mechanism or simply reflect limitations in the accessibility in densely packed, late replicating heterochromatin. In this context it is interesting to note that DNMT1 has distinctively slower FRAP recovery kinetics in late S phase (96). The observation that also HP1β is ubiquitinated by UHRF1 in S phase is novel and gives rise to speculations about possible functions in DNA replication and/or epigenetic regulation which are interesting starting points for future research.

Dysregulation of protein ubiquitination and degradation plays important roles in the development of human diseases (97,98). As several E3 ligases have been implicated in human cancer (99), the specific targeting of these enzymes is presently investigated as a less toxic alternative to current proteasomal inhibitors. However, high-throughput screening for inhibitors and modulators of E3 ubiquitin ligases mostly rely on cumbersome and costly biochemical assays and cell extracts based Ub-detection systems (100–103). Clearly, the most prominent ubiquitination target in cancer biology is the tumor suppressor p53. Ubiquitination by the E3 ligase HDM2 marks p53 for degradation and keeps its cellular levels low during normal cell cycle progression. Only upon DNA damage p53 levels increase to affect either cell cycle arrest or trigger apoptosis (104). To boost the activity of mutant p53 in tumor cells small molecules were screened to prevent p53 ubiquitination. Sophisticated and costly high-throughput screens eventually yielded Nutlin-3, which prevents p53 ubiquitination (60). We could detect the ubiquitination of p53 with our robust ubiF3Hc assay and monitor a drop in ubiquitination upon addition of Nutlin-3 with a simple optical readout in a multiwell format (Figure 7). As the ubiF3H assays are cell-based they provide besides the ubiquitination status of POIs also data on cell permeability, bioavailability and toxicity of candidate drugs and should, thus, be well suited for high-throughput and high-content drug screens.

In summary, we present a versatile ubiF3H assay to investigate the ubiquitination of specific proteins in live cells. We demonstrate that this simple assay is well suited to identify new targets, map ubiquitination sites, discriminate different types of ubiquitination, identify E3 ligases, proteases (DUBs) and inhibitors controlling the ubiquitination of specific proteins and monitor changes over time.

DATA AVAILABILITY

The data of flow cytometry experiments related to Figure 5F was submitted to the Flow Repository. The Repository URL for Referees is as follows, http://flowrepository.org/id/RvFrcVkKRpsNOJzvDRCcSAj2ccBKu6VvUttXYoXOYC7xyQflI04sS9BTCAmdf3mS.

The raw mass spectrometry proteomics data (Figure 1D) have been deposited at the ProteomeXchange with the dataset identifier 'PXD034335'.

REFERENCES

1. Hershko,A. and Ciechanover,A. (1998) The ubiquitin system. *Annu. Rev. Biochem.*, **67**, 425–479.
2. Komander,D. and Rape,M. (2012) The ubiquitin code. *Annu. Rev. Biochem.*, **81**, 203–229.
3. van Wijk,S.J., Fulda,S., Dikic,I. and Heilemann,M. (2019) Visualizing ubiquitination in mammalian cells. *EMBO Rep.*, **20**, e46520.
4. Coyaud,E., Mis,M., Laurent,E.M., Dunham,W.H., Couzens,A.L., Robitaille,M., Gingras,A.C., Angers,S. and Raught,B. (2015) BioID-based identification of skp cullin F-box (SCF)beta-TrCP1/2 E3 ligase substrates. *Mol. Cell. Proteomics*, **14**, 1781–1795.
5. Harper,J.W. and Tan,M.K. (2012) Understanding cullin-RING E3 biology through proteomics-based substrate identification. *Mol. Cell. Proteomics*, **11**, 1541–1550.
6. Merbl,Y., Refour,P., Patel,H., Springer,M. and Kirschner,M.W. (2013) Profiling of ubiquitin-like modifications reveals features of mitotic control. *Cell*, **152**, 1160–1172.
7. Batters,C., Zhu,H. and Sale,J.E. (2010) Visualisation of PCNA monoubiquitination in vivo by single pass spectral imaging FRET microscopy. *PLoS One*, **5**, e9008.
8. Ganesan,S., Ameer-Beg,S.M., Ng,T.T., Vojnovic,B. and Wouters,F.S. (2006) A dark yellow fluorescent protein (YFP)-based resonance energy-accepting chromoprotein (REACh) for forster resonance energy transfer with GFP. *Proc. Natl. Acad. Sci. U.S.A.*, **103**, 4089–4094.
9. Fang,D. and Kerppola,T.K. (2004) Ubiquitin-mediated fluorescence complementation reveals that jun ubiquitinated by itch/aip4 is localized to lysosomes. *Proc. Natl. Acad. Sci. U.S.A.*, **101**, 14782–14787.
10. Le Boulch,M., Brossard,A., Le Dez,G., Leon,S. and Rabut,G. (2020) Sensitive detection of protein ubiquitylation using a protein fragment complementation assay. *J. Cell Sci.*, **133**, jcs240093.
11. Levin-Kravets,O., Tanner,N., Shohat,N., Attali,I., Keren-Kaplan,T., Shusterman,A., Artzi,S., Varvak,A., Reshef,Y., Shi,X. *et al.* (2016) A bacterial genetic selection system for ubiquitylation cascade discovery. *Nat. Methods*, **13**, 945–952.
12. Emanuele,M.J., Elia,A.E., Xu,Q., Thoma,C.R., Izhar,L., Leng,Y., Guo,A., Chen,Y.N., Rush,J., Hsu,P.W. *et al.* (2011) Global identification of modular cullin-RING ligase substrates. *Cell*, **147**, 459–474.
13. Yen,H.C., Xu,Q., Chou,D.M., Zhao,Z. and Elledge,S.J. (2008) Global protein stability profiling in mammalian cells. *Science*, **322**, 918–923.
14. Riching,K.M., Mahan,S., Corona,C.R., McDougall,M., Vasta,J.D., Robers,M.B., Urh,M. and Daniels,D.L. (2018) Quantitative live-cell kinetic degradation and mechanistic profiling of PROTAC mode of action. *ACS Chem. Biol.*, **13**, 2758–2770.
15. Kim,W., Bennett,E.J., Huttlin,E.L., Guo,A., Li,J., Possemato,A., Sowa,M.E., Rad,R., Rush,J., Comb,M.J. *et al.* (2011) Systematic and quantitative assessment of the ubiquitin-modified proteome. *Mol. Cell*, **44**, 325–340.
16. Wagner,S.A., Beli,P., Weinert,B.T., Nielsen,M.L., Cox,J., Mann,M. and Choudhary,C. (2011) A proteome-wide, quantitative survey of in vivo ubiquitylation sites reveals widespread regulatory roles. *Mol. Cell. Proteomics*, **10**, M111 013284.
17. Xu,G., Paige,J.S. and Jaffrey,S.R. (2010) Global analysis of lysine ubiquitination by ubiquitin remnant immunoaffinity profiling. *Nat. Biotechnol.*, **28**, 868–873.
18. Hjerpe,R., Aillet,F., Lopitz-Otsoa,F., Lang,V., England,P. and Rodriguez,M.S. (2009) Efficient protection and isolation of ubiquitylated proteins using tandem ubiquitin-binding entities. *EMBO Rep.*, **10**, 1250–1258.
19. Mark,K.G., Loveless,T.B. and Toczyski,D.P. (2016) Isolation of ubiquitinated substrates by tandem affinity purification of E3 ligase-polyubiquitin-binding domain fusions (ligase traps). *Nat. Protoc.*, **11**, 291–301.
20. Husnjak,K. and Dikic,I. (2012) Ubiquitin-binding proteins: decoders of ubiquitin-mediated cellular functions. *Annu. Rev. Biochem.*, **81**, 291–322.
21. Raasi,S., Varadan,R., Fushman,D. and Pickart,C.M. (2005) Diverse polyubiquitin interaction properties of ubiquitin-associated domains. *Nat. Struct. Mol. Biol.*, **12**, 708–714.
22. Chen,Z., Zhong,Y., Wang,Y., Xu,S., Liu,Z., Baskakov,I.V., Monteiro,M.J., Karbowski,M., Shen,Y. and Fang,S. (2013) Ubiquitination-induced fluorescence complementation (UiFC) for detection of K48 ubiquitin chains in vitro and in live cells. *PLoS One*, **8**, e73482.
23. Sims,J.J., Scavone,F., Cooper,E.M., Kane,L.A., Youle,R.J., Boeke,J.D. and Cohen,R.E. (2012) Polyubiquitin-sensor proteins reveal localization and linkage-type dependence of cellular ubiquitin signaling. *Nat. Methods*, **9**, 303–309.
24. van Wijk,S.J., Fiskin,E., Putyrski,M., Pampaloni,F., Hou,J., Wild,P., Kensche,T., Grecco,H.E., Bastiaens,P. and Dikic,I. (2012) Fluorescence-based sensors to monitor localization and functions of linear and K63-linked ubiquitin chains in cells. *Mol. Cell*, **47**, 797–809.
25. Pohl,C. and Jentsch,S. (2009) Midbody ring disposal by autophagy is a post-abscission event of cytokinesis. *Nat. Cell Biol.*, **11**, 65–70.
26. Gao,Y., Li,Y., Zhang,C., Zhao,M., Deng,C., Lan,Q., Liu,Z., Su,N., Wang,J., Xu,F. *et al.* (2016) Enhanced purification of ubiquitinated proteins by engineered tandem hybrid Ubiquitin-binding domains (ThUBDs). *Mol. Cell. Proteomics*, **15**, 1381–1396.
27. Lopitz-Otsoa,F., Rodriguez-Suarez,E., Aillet,F., Casado-Vela,J., Lang,V., Matthiesen,R., Elortza,F. and Rodriguez,M.S. (2012) Integrative analysis of the ubiquitin proteome isolated using tandem ubiquitin binding entities (TUBEs). *J. Proteomics*, **75**, 2998–3014.
28. Meilinger,D., Fellinger,K., Bultmann,S., Rothbauer,U., Bonapace,I.M., Klinkert,W.E., Spada,F. and Leonhardt,H. (2009) Np95 interacts with de novo DNA methyltransferases, dnmt3a and dnmt3b, and mediates epigenetic silencing of the viral CMV promoter in embryonic stem cells. *EMBO Rep.*, **10**, 1259–1264.
29. Qin,W., Leonhardt,H. and Spada,F. (2011) Usp7 and uhrf1 control ubiquitination and stability of the maintenance DNA methyltransferase dnmt1. *J. Cell. Biochem.*, **112**, 439–444.
30. Qin,W., Wolf,P., Liu,N., Link,S., Smets,M., La Mastra,F., Forne,I., Pichler,G., Horl,D., Fellinger,K. *et al.* (2015) DNA methylation requires a DNMT1 ubiquitin interacting motif (UIM) and histone ubiquitination. *Cell Res.*, **25**, 911–929.

31. Easwaran,H.P., Schermelleh,L., Leonhardt,H. and Cardoso,M.C. (2004) Replication-independent chromatin loading of dnmt1 during G2 and m phases. *EMBO Rep.*, **5**, 1181–1186.

32. Herce,H.D., Deng,W., Helma,J., Leonhardt,H. and Cardoso,M.C. (2013) Visualization and targeted disruption of protein interactions in living cells. *Nat. Commun.*, **4**, 2660.

33. Rothbauer,U., Zolghadr,K., Muyldermans,S., Schepers,A., Cardoso,M.C. and Leonhardt,H. (2008) A versatile nanotrap for biochemical and functional studies with fluorescent fusion proteins. *Mol. Cell. Proteomics*, **7**, 282–289.

34. Kirchhofer,A., Helma,J., Schmidthals,K., Frauer,C., Cui,S., Karcher,A., Pellis,M., Muyldermans,S., Casas-Delucchi,C.S., Cardoso,M.C. *et al.* (2010) Modulation of protein properties in living cells using nanobodies. *Nat. Struct. Mol. Biol.*, **17**, 133–138.

35. Tsukamoto,T., Hashiguchi,N., Janicki,S.M., Tumbar,T., Belmont,A.S. and Spector,D.L. (2000) Visualization of gene activity in living cells. *Nat. Cell Biol.*, **2**, 871–878.

36. Schermelleh,L., Haemmer,A., Spada,F., Rosing,N., Meilinger,D., Rothbauer,U., Cardoso,M.C. and Leonhardt,H. (2007) Dynamics of dnmt1 interaction with the replication machinery and its role in postreplicative maintenance of DNA methylation. *Nucleic Acids Res.*, **35**, 4301–4312.

37. Krude,T. (1999) Mimosine arrests proliferating human cells before onset of DNA replication in a dose-dependent manner. *Exp. Cell. Res.*, **247**, 148–159.

38. Szuts,D. and Krude,T. (2004) Cell cycle arrest at the initiation step of human chromosomal DNA replication causes DNA damage. *J. Cell Sci.*, **117**, 4897–4908.

39. Chagin,V.O., Casas-Delucchi,C.S., Reinhart,M., Schermelleh,L., Markaki,Y., Maiser,A., Bolius,J.J., Bensimon,A., Fillies,M., Domaing,P. *et al.* (2016) 4D Visualization of replication foci in mammalian cells corresponding to individual replicons. *Nat. Commun.*, **7**, 11231.

40. Qin,W., Ugur,E., Mulholland,C.B., Bultmann,S., Solovei,I., Modic,M., Smets,M., Wierer,M., Forne,I., Imhof,A. *et al.* (2021) Phosphorylation of the HP1beta hinge region sequesters KAP1 in heterochromatin and promotes the exit from naive pluripotency. *Nucleic Acids Res.*, **49**, 7406–7423.

41. Park,S.H., Kukushkin,Y., Gupta,R., Chen,T., Konagai,A., Hipp,M.S., Hayer-Hartl,M. and Hartl,F.U. (2013) PolyQ proteins interfere with nuclear degradation of cytosolic proteins by sequestering the sis1p chaperone. *Cell*, **154**, 134–145.

42. Shevchenko,A., Loboda,A., Shevchenko,A., Ens,W. and Standing,K.G. (2000) MALDI quadrupole time-of-flight mass spectrometry: a powerful tool for proteomic research. *Anal. Chem.*, **72**, 2132–2141.

43. Wilm,M. and Mann,M. (1996) Analytical properties of the nanoelectrospray ion source. *Anal. Chem.*, **68**, 1–8.

44. Chagin,V.O., Reinhart,B., Becker,A., Mortusewicz,O., Jost,K.L., Rapp,A., Leonhardt,H. and Cardoso,M.C. (2019) Processive DNA synthesis is associated with localized decompaction of constitutive heterochromatin at the sites of DNA replication and repair. *Nucleus*, **10**, 231–253.

45. Schindelin,J., Arganda-Carreras,I., Frise,E., Kaynig,V., Longair,M., Pietzsch,T., Preibisch,S., Rueden,C., Saalfeld,S., Schmid,B. *et al.* (2012) Fiji: an open-source platform for biological-image analysis. *Nat. Methods*, **9**, 676–682.

46. Schneider,C.A., Rasband,W.S. and Eliceiri,K.W. (2012) NIH image to imagej: 25 years of image analysis. *Nat. Methods*, **9**, 671–675.

47. Qin,W., Stengl,A., Ugur,E., Leidescher,S., Ryan,J., Cardoso,M.C. and Leonhardt,H. (2021) HP1beta carries an acidic linker domain and requires H3K9me3 for phase separation. *Nucleus*, **12**, 44–57.

48. Citterio,E., Papait,R., Nicassio,F., Vecchi,M., Gomiero,P., Mantovani,R., Di Fiore,P.P. and Bonapace,I.M. (2004) Np95 is a histone-binding protein endowed with ubiquitin ligase activity. *Mol. Cell. Biol.*, **24**, 2526–2535.

49. Bertolaet,B.L., Clarke,D.J., Wolff,M., Watson,M.H., Henze,M., Divita,G. and Reed,S.I. (2001) UBA domains of DNA damage-inducible proteins interact with ubiquitin. *Nat. Struct. Biol.*, **8**, 417–422.

50. Choi,Y.S., Bollinger,S.A., Prada,L.F., Scavone,F., Yao,T. and Cohen,R.E. (2019) High-affinity free ubiquitin sensors for quantifying ubiquitin homeostasis and deubiquitination. *Nat. Methods*, **16**, 771–777.

51. Bostick,M., Kim,J.K., Esteve,P.O., Clark,A., Pradhan,S. and Jacobsen,S.E. (2007) UHRF1 plays a role in maintaining DNA methylation in mammalian cells. *Science*, **317**, 1760–1764.

52. Nishiyama,A., Yamaguchi,L., Sharif,J., Johmura,Y., Kawamura,T., Nakanishi,K., Shimamura,S., Arita,K., Kodama,T., Ishikawa,F. *et al.* (2013) Uhrf1-dependent H3K23 ubiquitylation couples maintenance DNA methylation and replication. *Nature*, **502**, 249–253.

53. Sharif,J., Muto,M., Takebayashi,S., Suetake,I., Iwamatsu,A., Endo,T.A., Shinga,J., Mizutani-Koseki,Y., Toyoda,T., Okamura,K. *et al.* (2007) The SRA protein Np95 mediates epigenetic inheritance by recruiting dnmt1 to methylated DNA. *Nature*, **450**, 908–912.

54. Cheng,J., Li,Z., Gong,R., Fang,J., Yang,Y., Sun,C., Yang,H. and Xu,Y. (2015) Molecular mechanism for the substrate recognition of USP7. *Protein Cell*, **6**, 849–852.

55. Cheng,J., Yang,H., Fang,J., Ma,L., Gong,R., Wang,P., Li,Z. and Xu,Y. (2015) Molecular mechanism for USP7-mediated DNMT1 stabilization by acetylation. *Nat. Commun.*, **6**, 7023.

56. Du,Z., Song,J., Wang,Y., Zhao,Y., Guda,K., Yang,S., Kao,H.Y., Xu,Y., Willis,J., Markowitz,S.D. *et al.* (2010) DNMT1 stability is regulated by proteins coordinating deubiquitination and acetylation-driven ubiquitination. *Sci. Signal*, **3**, ra80.

57. Karg,E., Smets,M., Ryan,J., Forne,I., Qin,W., Mulholland,C.B., Kalideris,G., Imhof,A., Bultmann,S. and Leonhardt,H. (2017) Ubiquitome analysis reveals PCNA-Associated factor 15 (PAF15) as a specific ubiquitination target of UHRF1 in embryonic stem cells. *J. Mol. Biol.*, **429**, 3814–3824.

58. Nishiyama,A., Mulholland,C.B., Bultmann,S., Kori,S., Endo,A., Saeki,Y., Qin,W., Trummer,C., Chiba,Y., Yokoyama,H. *et al.* (2020) Two distinct modes of DNMT1 recruitment ensure stable maintenance DNA methylation. *Nat. Commun.*, **11**, 1222.

59. Haupt,Y., Maya,R., Kazaz,A. and Oren,M. (1997) Mdm2 promotes the rapid degradation of p53. *Nature*, **387**, 296–299.

60. Vassilev,L.T., Vu,B.T., Graves,B., Carvajal,D., Podlaski,F., Filipovic,Z., Kong,N., Kammlott,U., Lukacs,C., Klein,C. *et al.* (2004) In vivo activation of the p53 pathway by small-molecule antagonists of MDM2. *Science*, **303**, 844–848.

61. Kawaguchi,K., Uo,K., Tanaka,T. and Komada,M. (2017) Tandem UIMs confer lys48 ubiquitin chain substrate preference to deubiquitinase USP25. *Sci. Rep.*, **7**, 45037.

62. Kulathu,Y., Akutsu,M., Bremm,A., Hofmann,K. and Komander,D. (2009) Two-sided ubiquitin binding explains specificity of the TAB2 NZF domain. *Nat. Struct. Mol. Biol.*, **16**, 1328–1330.

63. Zhang,N., Wang,Q., Ehlinger,A., Randles,L., Lary,J.W., Kang,Y., Haririnia,A., Storaska,A.J., Cole,J.L., Fushman,D. *et al.* (2009) Structure of the s5a:k48-linked diubiquitin complex and its interactions with rpn13. *Mol. Cell*, **35**, 280–290.

64. Yu,J., Qin,B., Moyer,A.M., Nowsheen,S., Liu,T., Qin,S., Zhuang,Y., Liu,D., Lu,S.W., Kalari,K.R. *et al.* (2018) DNA methyltransferase expression in triple-negative breast cancer predicts sensitivity to decitabine. *J. Clin. Invest.*, **128**, 2376–2388.

65. Deng,T., Yan,G., Song,X., Xie,L., Zhou,Y., Li,J., Hu,X., Li,Z., Hu,J., Zhang,Y. *et al.* (2018) Deubiquitylation and stabilization of p21 by USP11 is critical for cell-cycle progression and DNA damage responses. *Proc. Natl. Acad. Sci. U.S.A.*, **115**, 4678–4683.

66. Tsuruta,F., Takebe,A., Haratake,K., Kanemori,Y., Kim,J., Endo,T., Kigoshi,Y., Fukuda,T., Miyahara,H., Ebina,M. *et al.* (2016) SCFFbl12 increases p21Waf1/Cip1 expression level through atypical ubiquitin chain synthesis. *Mol. Cell. Biol.*, **36**, 2182–2194.

67. Jin,L., Williamson,A., Banerjee,S., Philipp,I. and Rape,M. (2008) Mechanism of ubiquitin-chain formation by the human anaphase-promoting complex. *Cell*, **133**, 653–665.

68. Hock,A.K. and Vousden,K.H. (2014) The role of ubiquitin modification in the regulation of p53. *Biochim. Biophys. Acta*, **1843**, 137–149.

69. Stewart,G.S., Panier,S., Townsend,K., Al-Hakim,A.K., Kolas,N.K., Miller,E.S., Nakada,S., Ylanko,J., Olivarius,S., Mendez,M. *et al.* (2009) The RIDDLE syndrome protein mediates a ubiquitin-dependent signaling cascade at sites of DNA damage. *Cell*, **136**, 420–434.

70. Zhou,W., Zhu,P., Wang,J., Pascual,G., Ohgi,K.A., Lozach,J., Glass,C.K. and Rosenfeld,M.G. (2008) Histone H2A monoubiquitination represses transcription by inhibiting RNA polymerase II transcriptional elongation. *Mol. Cell*, **29**, 69–80.

71. Bekker-Jensen,S., Rendtlew Danielsen,J., Fugger,K., Gromova,I., Nerstedt,A., Lukas,C., Bartek,J., Lukas,J. and Mailand,N. (2010) HERC2 coordinates ubiquitin-dependent assembly of DNA repair factors on damaged chromosomes. *Nat. Cell Biol.*, **12**, 80–86.

72. Elia,A.E., Boardman,A.P., Wang,D.C., Huttlin,E.L., Everley,R.A., Dephoure,N., Zhou,C., Koren,I., Gygi,S.P. and Elledge,S.J. (2015) Quantitative proteomic atlas of ubiquitination and acetylation in the DNA damage response. *Mol. Cell*, **59**, 867–881.

73. Thorslund,T., Ripplinger,A., Hoffmann,S., Wild,T., Uckelmann,M., Villumsen,B., Narita,T., Sixma,T.K., Choudhary,C., Bekker-Jensen,S. *et al.* (2015) Histone H1 couples initiation and amplification of ubiquitin signalling after DNA damage. *Nature*, **527**, 389–393.

74. Acs,K., Luijsterburg,M.S., Ackermann,L., Salomons,F.A., Hoppe,T. and Dantuma,N.P. (2011) The AAA-ATPase VCP/p97 promotes 53BP1 recruitment by removing L3MBTL1 from DNA double-strand breaks. *Nat. Struct. Mol. Biol.*, **18**, 1345–1350.

75. Ali,M.A.M., Strickfaden,H., Lee,B.L., Spyracopoulos,L. and Hendzel,M.J. (2018) RYBP is a K63-Ubiquitin-Chain-Binding protein that inhibits homologous recombination repair. *Cell Rep.*, **22**, 383–395.

76. Feng,L. and Chen,J. (2012) The E3 ligase RNF8 regulates KU80 removal and NHEJ repair. *Nat. Struct. Mol. Biol.*, **19**, 201–206.

77. Mallette,F.A., Mattiroli,F., Cui,G., Young,L.C., Hendzel,M.J., Mer,G., Sixma,T.K. and Richard,S. (2012) RNF8- and RNF168-dependent degradation of KDM4A/JMJD2A triggers 53BP1 recruitment to DNA damage sites. *EMBO J.*, **31**, 1865–1878.

78. Meerang,M., Ritz,D., Paliwal,S., Garajova,Z., Bosshard,M., Mailand,N., Janscak,P., Hubscher,U., Meyer,H. and Ramadan,K. (2011) The ubiquitin-selective segregase VCP/p97 orchestrates the response to DNA double-strand breaks. *Nat. Cell Biol.*, **13**, 1376–1382.

79. Chau,V., Tobias,J.W., Bachmair,A., Marriott,D., Ecker,D.J., Gonda,D.K. and Varshavsky,A. (1989) A multiubiquitin chain is confined to specific lysine in a targeted short-lived protein. *Science*, **243**, 1576–1583.

80. Hu,C.D. and Kerppola,T.K. (2003) Simultaneous visualization of multiple protein interactions in living cells using multicolor fluorescence complementation analysis. *Nat. Biotechnol.*, **21**, 539–545.

81. Yamaguchi,L., Nishiyama,A., Misaki,T., Johmura,Y., Ueda,J., Arita,K., Nagao,K., Obuse,C. and Nakanishi,M. (2017) Usp7-dependent histone H3 deubiquitylation regulates maintenance of DNA methylation. *Sci. Rep.*, **7**, 55.

82. Leonhardt,H., Rahn,H.P., Weinzierl,P., Sporbert,A., Cremer,T., Zink,D. and Cardoso,M.C. (2000) Dynamics of DNA replication factories in living cells. *J. Cell Biol.*, **149**, 271–280.

83. Foster,B.M., Stolz,P., Mulholland,C.B., Montoya,A., Kramer,H., Bultmann,S. and Bartke,T. (2018) Critical role of the UBL domain in stimulating the E3 ubiquitin ligase activity of UHRF1 toward chromatin. *Mol. Cell*, **72**, 739–752.

84. Sales-Gil,R. and Vagnarelli,P. (2020) How HP1 post-translational modifications regulate heterochromatin formation and maintenance. *Cells*, **9**, 1460.

85. Zolghadr,K., Mortusewicz,O., Rothbauer,U., Kleinhans,R., Goehler,H., Wanker,E.E., Cardoso,M.C. and Leonhardt,H. (2008) A fluorescent two-hybrid assay for direct visualization of protein interactions in living cells. *Mol. Cell. Proteomics*, **7**, 2279–2287.

86. Mulholland,C.B., Smets,M., Schmidtmann,E., Leidescher,S., Markaki,Y., Hofweber,M., Qin,W., Manzo,M., Kremmer,E.,

Thanisch,K. *et al.* (2015) A modular open platform for systematic functional studies under physiological conditions. *Nucleic Acids Res.*, **43**, e112.

87. Michel,M.A., Swatek,K.N., Hospenthal,M.K. and Komander,D. (2017) Ubiquitin linkage-specific affimers reveal insights into K6-Linked ubiquitin signaling. *Mol. Cell*, **68**, 233–246.

88. Schwertman,P., Bekker-Jensen,S. and Mailand,N. (2016) Regulation of DNA double-strand break repair by ubiquitin and ubiquitin-like modifiers. *Nat. Rev. Mol. Cell Biol.*, **17**, 379–394.

89. Cheutin,T., McNairn,A.J., Jenuwein,T., Gilbert,D.M., Singh,P.B. and Misteli,T. (2003) Maintenance of stable heterochromatin domains by dynamic HP1 binding. *Science*, **299**, 721–725.

90. Kimura,H. and Cook,P.R. (2001) Kinetics of core histones in living human cells: little exchange of H3 and H4 and some rapid exchange of H2B. *J. Cell Biol.*, **153**, 1341–1353.

91. Filonov,G.S. and Verkhusha,V.V. (2013) A near-infrared BiFC reporter for in vivo imaging of protein-protein interactions. *Chem. Biol.*, **20**, 1078–1086.

92. Shyu,Y.J. and Hu,C.D. (2008) Fluorescence complementation: an emerging tool for biological research. *Trends Biotechnol.*, **26**, 622–630.

93. Anderie,I. and Schmid,A. (2007) In vivo visualization of actin dynamics and actin interactions by BiFC. *Cell Biol. Int.*, **31**, 1131–1135.

94. Guo,Y., Rebecchi,M. and Scarlata,S. (2005) Phospholipase cbeta2 binds to and inhibits phospholipase cdelta1. *J. Biol. Chem.*, **280**, 1438–1447.

95. Schmidt,C., Peng,B., Li,Z., Sclabas,G.M., Fujioka,S., Niu,J., Schmidt-Supprian,M., Evans,D.B., Abbruzzese,J.L. and Chiao,P.J. (2003) Mechanisms of proinflammatory cytokine-induced biphasic NF-kappaB activation. *Mol. Cell*, **12**, 1287–1300.

96. Schneider,K., Fuchs,C., Dobay,A., Rottach,A., Qin,W., Wolf,P., Alvarez-Castro,J.M., Nalaskowski,M.M., Kremmer,E., Schmid,V. *et al.* (2013) Dissection of cell cycle-dependent dynamics of dnmt1 by FRAP and diffusion-coupled modeling. *Nucleic Acids Res.*, **41**, 4860–4876.

97. Popovic,D., Vucic,D. and Dikic,I. (2014) Ubiquitination in disease pathogenesis and treatment. *Nat. Med.*, **20**, 1242–1253.

98. Roeten,M.S.F., Cloos,J. and Jansen,G. (2018) Positioning of proteasome inhibitors in therapy of solid malignancies. *Cancer Chemother. Pharmacol.*, **81**, 227–243.

99. Senft,D., Qi,J. and Ronai,Z.A. (2018) Ubiquitin ligases in oncogenic transformation and cancer therapy. *Nat. Rev. Cancer*, **18**, 69–88.

100. Franklin,T.G. and Pruneda,J.N. (2019) A high-throughput assay for monitoring ubiquitination in real time. *Front Chem*, **7**, 816.

101. Rossi,M., Rotblat,B., Ansell,K., Amelio,I., Caraglia,M., Misso,G., Bernassola,F., Cavasotto,C.N., Knight,R.A., Ciechanover,A. *et al.* (2014) High throughput screening for inhibitors of the HECT ubiquitin E3 ligase ITCH identifies antidepressant drugs as regulators of autophagy. *Cell Death. Dis.*, **5**, e1203.

102. Sun,Y. (2005) Overview of approaches for screening for ubiquitin ligase inhibitors. *Methods Enzymol.*, **399**, 654–663.

103. Tian,M., Zeng,T., Liu,M., Han,S., Lin,H., Lin,Q., Li,L., Jiang,T., Li,G., Lin,H. *et al.* (2019) A cell-based high-throughput screening method based on a ubiquitin-reference technique for identifying modulators of E3 ligases. *J. Biol. Chem.*, **294**, 2880–2891.

104. Lakin,N.D. and Jackson,S.P. (1999) Regulation of p53 in response to DNA damage. *Oncogene*, **18**, 7644–7655.